Biosorption of Procion Magenta and Black Azabache Textile Dyes using Banana and Carrot Peel Waste: A Comparative Analysis of Pure and Blended Systems

Samiksha B. Patil, Richa Singh

Department of Biotechnology, SIES College of Arts, Science and Commerce (Autonomous), Sion (W), Mumbai, India

---

Acknowledgement:

The Version of Record of this manuscript has been published and is available in *International Journal of Phytoremediation*, 23 April 2026, http://www.tandfonline.com/10.1080/15226514.2026.2660151

DOI: https://doi.org/10.1080/15226514.2026.2660151
Journal: International Journal of Phytoremediation (Int. J. Phytoremediation)

Biosorption of Procion Magenta and Black Azabache Textile Dyes using Banana and Carrot Peel Waste: A Comparative Analysis of Pure and Blended Systems

Samiksha B. Patil[a] and Richa Singh[a]*

[a]*Department of Biotechnology, SIES College of Arts, Science and Commerce (Autonomous), Sion (W), Mumbai, India*

ORCID : SP (http://orcid.org/0009-0002-5243-9253); **RS** (http://orcid.org/0000-0001-7184-9958)

***Corresponding author:**

Dr. Richa Singh (richasngh316@gmail.com / richas@sies.edu.in)

Statement of Novelty

This study presents the first systematic comparative evaluation of biosorption of a pure reactive dye (Procion MX Magenta) and a commercial blended dye (Black Azabache) using banana and carrot peel wastes. While biosorption studies predominantly address individual dyes, the adsorption of commercial dye blends remains largely unexplored. This work demonstrates that dye complexity influences functional group interactions and adsorption behavior, revealing distinct mechanisms for pure and blended dyes. By collectively analyzing four dye–biosorbent systems, the study provides new mechanistic insights into dye-biosorbent interactions and reusability, thereby advancing the existing understanding of dye removal processes using sustainable waste-derived materials.

Abstract

The textile industry generates large volumes of toxic dye-laden wastewater, necessitating sustainable treatment strategies. This study presents the first comparative evaluation of the adsorption of a pure dye, Procion MX Magenta (PM), and a blended dye, Black Azabache (RB), using banana and carrot peel waste as low-cost biosorbents. Optimal biosorption occurred at a dye concentration of 100 mg L^{-1} using 2% biosorbent at pH 2 within 60 min, resulting in >70% dye removal. Adsorption capacities of biosorbents ranged from 8.7 to 36.6 mg g^{-1}. Kinetic studies demonstrated that dye uptake followed a pseudo-second-order model (R^2>0.9). Isotherm analysis revealed that adsorption on banana followed the Freundlich model, whereas RB-carrot peel data did not conform to any conventional isotherm model, indicating more complex adsorption behavior in the blended dye system. FTIR, SEM, and BET analyses confirmed pore-filling and surface binding of the dye mediated by weak interactions involving hydroxyl, carboxyl, amine, and aromatic functional groups. Acidic regeneration of immobilized biosorbent enabled its effective reuse over five successive cycles, highlighting a sustainable and efficient approach for dye removal coupled with domestic waste valorization.

Keywords

Agro-waste, Adsorption, Optimization, Isotherm, Immobilization, Regeneration

Introduction

The textile industry is a major consumer of water and chemical dyes. More than 10,000 types of dyes and pigments are used in these industries for dyeing and finishing processes (Singh *et al.,* 2024). A daily production of 50,000 meters of fabric can use up to 1–2 million litres of water, thereby producing large volumes of wastewater contaminated with residual colorants, diluted solids, suspended particles, and toxic metals (Islam *et al.* 2022; Kumari *et al.* 2024). The dye concentration in these wastewaters ranges from 10 to 7000 mg L^{-1}, depending on the nature of the textile industry and the treatment procedures (Yaseen and Scholz 2019).

Synthetic dyes, such as acid, reactive, direct, and azo dyes, are an excellent choice for fabric dyeing nowadays as they resist fading and degradation. However, these same properties make them environmentally persistent, posing serious health risks. Their release into water bodies harms aquatic ecosystems by hindering photosynthesis and reducing dissolved oxygen levels, which disrupts food chains (Mehra *et al.* 2021; Singha *et al.* 2021). Moreover, synthetic dyes contain aromatic amines, naphthol derivatives, sulphur and heavy metals like mercury, lead, and chromium. Such hazardous compounds are reported to be toxic, mutagenic, endocrine-disrupting, and potentially carcinogenic (Hemashenpagam and Selvajeyanthi 2023; Girija and Mareeswaran 2023; Singha *et al.* 2021). Exposure to these dyes through contaminated water has also been linked to skin irritation, respiratory issues, genetic mutations, and other health problems in humans (Pokharia and Ahluwalia 2015; Islam *et al.* 2022).

Conventional wastewater treatment methods include coagulation, flocculation, oxidation, membrane filtration, chemical treatment, and activated carbon adsorption (Bouchelkia *et al.* 2016; Kumari *et al.* 2024). Although effective to varying degrees, these methods often suffer from limitations, including high operational and maintenance costs, energy-intensive processes, membrane fouling, and generation of secondary pollutants, such

as toxic sludge (Peng and Guo 2020; Shamshad and Rehman 2025). Therefore, there is a need for low-cost, efficient, and sustainable alternatives for large-scale dye removal.

Biosorption has emerged as an environmentally friendly and economically viable approach. It primarily relies on physicochemical interactions between dye molecules and diverse functional groups present on biomass surfaces. The process is non-destructive, can be carried out under mild conditions, and often exhibits excellent dye removal efficiencies owing to high surface area and abundant functional groups (Aksu 2005). Domestic, agricultural, and agro-industrial wastes are particularly promising for biosorption due to their abundance, low cost, easy availability, and biodegradability (Akpomie and Conradie 2020; Vievard *et al.* 2023). Utilizing these waste materials not only provides an efficient route for dye removal but also supports waste valorization and circular-economy objectives. Numerous studies have reported the potential of phytobiomass, such as orange peel, potato peel, cactus fruit, rice straw, artichoke, aloe vera leaves, etc., in removing individual synthetic dyes (Akkari *et al.* 2024; Chahal *et al.* 2024; Djama *et al.* 2023; Gupta *et al.* 2025; Kumari *et al.* 2023; Yarik *et al.* 2025) or heavy metals (Gómez-Aguilar *et al.* 2022; Hastuti *et al.* 2018; Raji *et al.* 2025).

Banana and carrot peels are among the most commonly generated household food wastes and possess a rich biochemical composition. Banana peels have lignin, cellulose, hemicellulose, and pectin, which provide numerous hydroxyl and carboxyl groups capable of binding dye molecules (Khawas *et al.* 2017). Similarly, carrot peels are reported to contain carotenoids, phenolics, and pectin, which facilitate the binding through both physical and chemical adsorption mechanisms (Hastuti *et al.* 2018; Jayesree *et al.* 2021). Their natural porosity and surface functionality make them suitable candidates for removing both cationic and anionic dyes from aqueous solutions (Akpomie and Conradie 2020). Application of these peel wastes has been reported in the effective removal of dyes, such as methylene blue (Hashem

et al. 2020), malachite green, rhodamine B (Nasra *et al.* 2021), congo red (Daffalla *et al.* 2024), and reactive dyes (Akter *et al.* 2021; Kapoor *et al.* 2022; Yasmeen *et al.* 2025). While both materials have been individually explored for the removal of selected individual dyes, a direct comparative study evaluating their relative performance, mechanisms, and suitability for different dye systems is not available.

Another critical gap in existing literature is the lack of studies addressing commercial dye blends. Since most modern fabrics are blends, the textile industry relies heavily on binary/ternary dye blends or proprietary dye mixtures. Due to the presence of multiple chromophores and functional groups, these dye blends provide uniform and water-fast color to the fabric (Ibrahim 2011; Elsisi *et al.* 2025). Despite this, most adsorption studies are based on individual pure dyes (Akter *et al.* 2021; Kapoor *et al.* 2022; Munagapati *et al.* 2018; Yasmeen *et al.* 2025). Furthermore, the blended dyes may exhibit adsorption behavior that differs from that of single-component systems due to synergistic or competitive interactions (Meretoudi *et al.* 2025). Hence, adsorption studies on dye blends are critical for accurately reflecting treatment efficiency and removal mechanisms.

In this context, the present study focuses on the removal of two commercial textile dyes, Procion MX Magenta and Black Azabache, with contrasting characteristics. Procion MX Magenta is a pure fibre-reactive monoazo dye widely used in the textile industry. The dye binds to cotton and cellulosic fibres through covalent bonds. However, its reactive groups and sulfonated structure make it resistant to degradation, leading to persistence in wastewater (Aksu 2005). Black Azabache, on the other hand, is a proprietary commercial all-purpose dye blend powder suitable for a wide range of fabrics, such as cotton, linen, hemp, silk, wool, rayon, and nylon. The dye is also commonly available for household dyeing (Rit 2025). Due to its easy consumer accessibility, its discharge into domestic wastewater also contributes to dye pollution.

Hence, removal of these dyes is crucial to mitigate their adverse impacts on human health and the environment. Despite numerous reports on biosorption-based dye removal, no prior study has investigated the comparative biosorption of Procion MX Magenta and Black Azabache using banana and carrot peel waste as biosorbents. Furthermore, differences in adsorption behavior between pure dyes and commercial blends, as well as between distinct biosorbents, remain poorly understood. Addressing these gaps is essential to advance the application of waste-derived biosorbents in wastewater treatment.

In view of this, the primary objective of this study is to evaluate and compare the biosorption of the reactive dye Procion MX Magenta and the commercial dye blend Black Azabache using banana and carrot peel powders. In addition, it investigates the influence of key operational parameters on dye uptake and adsorption mechanisms through various adsorption models and physicochemical characterization. It further assesses the reusability of the biosorbent via immobilization and sorption–desorption cycles. The comparative evaluation, mechanistic insights, and reusability assessment demonstrate the practical potential of domestic waste materials for sustainable dye removal, thereby enhancing the environmental relevance of the study.

Materials and methods

Chemicals

Calcium chloride ($CaCl_2$, 98%), sodium alginate (91%), hydrochloric acid (HCl, 37%), and sodium hydroxide (NaOH, 97%), were procured from Loba Chemie, India. Textile dyes, Jacquard® Procion MX 034 Magenta (PM) and Rit® Black Azabache (RB), were purchased from a local dyeing market in Mumbai, India. The exact chemical composition and purity are not disclosed by the manufacturers, as is typical for commercial dyes. The dyes were used as received.

Preparation of biosorbent

Fresh carrot (*Daucus carota sativus*) and banana (*Musa paradisiaca Linn*) peels were collected from domestic waste. The peels were thoroughly washed with tap water, followed by distilled water. The washed material was then cut into small pieces and dried in a hot air oven at 50°C overnight. The dried material was ground using an electric blender and filtered through a sieve (mesh size 0.3 mm) to obtain a fine powder of ≤300 µm. The powdered biosorbent was stored in airtight bottles to protect it from moisture.

Absorbance maxima of dyes

Appropriate weights of both the dyes, RB and PM, were dissolved in distilled water to obtain a stock solution of 100 mg L^{-1}. UV-Visible spectra of the dyes were recorded over the range 400-800 nm using a UV-Visible Spectrophotometer (Equip-Tronics EQ-825A, India) to determine their absorbance maxima (λ_{max}). Standard calibration curves were prepared by making a series of concentrations of each dye ranging from 1 to 100 mg L^{-1} and recording the absorbance at their corresponding λ_{max}. The linearity of the calibration curves was confirmed with correlation coefficients (R^2). The regression equations thus obtained were used to estimate residual dye concentrations in subsequent experiments.

Effect of operational parameters

In a typical experiment, 0.5 g of banana and carrot peel powder was suspended in 50 ml (equivalent to 1% w/v) of 100 mg L^{-1} of dye solution in Erlenmeyer flasks to make four separate systems: banana with PM (BPM), banana with RB (BRB), carrot with PM (CPM), and carrot with RB (CRB). The initial pH of the dye solution was maintained at natural pH (6.8±0.2). The reaction mixture was agitated continuously at 150 rpm in an orbital shaker (Labline, India) at 25±2ºC. To optimize the operational parameters, a series of batch biosorption studies was

conducted by varying contact time (10–60 min), biosorbent concentration (1–3%, w/v), pH (2–10), and initial dye concentration (up to 150 mg L^{-1}). At a pre-determined time interval, aliquots were withdrawn, followed by centrifugation (Remi R-8C, India) at 2,000 rpm for 5 min to separate the biosorbent. The supernatant was further filtered through Whatman No. 1 paper (pre-wetted with distilled water to minimize dye retention) to remove any remaining fine suspended particles. The absorbance of the filtrate was recorded at the corresponding λ_{max} of the respective dye solution. The residual dye concentration in the supernatant was determined from the respective calibration curves. Percentage biosorption was calculated using Equation (1):

$$\text{Biosorption (\%)} = \left(\frac{C_i - C_f}{C_i}\right) \times 100, \quad (1)$$

where, C_i and C_f are the initial and final dye concentration (mg L^{-1}). Suitable controls were maintained. All experiments were performed in triplicate, and values were expressed as mean ± s.d.

Characterization of biosorbent

Point of zero charge (pH_{PZC})

pH_{PZC} of both the banana and carrot peel biosorbents was determined using the pH drift method (Daffalla *et al.* 2024). A 2% (w/v) biosorbent suspension was prepared by adding 1 g of the biosorbent to 50 ml of aqueous solution, with the initial pH adjusted between 2 and 10 using 1N HCl and 1N NaOH. The suspensions were incubated on the shaker at 150 rpm / 25±2ºC for 60 min, after which the final pH was recorded using a calibrated pH meter (HM Digital pH-80, India). The pH_{PZC} was determined from the point where the difference between the initial and final pH values (ΔpH) approached zero.

Fourier Transform Infrared Spectroscopy (FTIR)

The infrared spectra of the dried biosorbents, before and after biosorption at optimized conditions, were recorded using an FTIR spectrometer (Bruker Vertex 80, Germany) to identify the functional groups involved in dye biosorption. Spectra were collected over the range of 4000–400 cm^{-1} at a resolution of 0.2 cm^{-1} with 32 scans per sample. Samples were prepared using the KBr pellet method, and baseline correction was applied prior to analysis.

Scanning Electron Microscope (SEM) and Energy Dispersive X-ray (EDX)

Dried biosorbent samples, before and after dye adsorption, were mounted on aluminium stubs using double-sided carbon adhesive tape, followed by sputter-coating (Mascotek Scientific SC-180RLite, India) with a thin conductive layer of gold. The surface morphology of the samples was examined using SEM (Zeiss Evo 80, India). Images were recorded using a secondary electron detector at an accelerating voltage of 20.00 kV. Micrographs were acquired at different magnifications, with representative images recorded at 3.00 to 5.00 K X. EDX was carried out in conjunction with SEM and the corresponding spectra were collected from selected regions of the SEM micrographs for elemental confirmation.

Surface area and pore size analysis

Specific surface area and pore structure of the biosorbents were determined by nitrogen adsorption-desorption, measurements recorded at 77.35 K, using a surface area analyzer (Quantachrome NOVAtouch 2LX, India). Prior to analysis, all samples were degassed at 120°C for 3 h under vacuum to remove physically adsorbed moisture and volatile impurities. Brunauer- Emmett-Teller (BET) surface area was obtained from the adsorption branch using the multi-point method ($P/P_0 \approx 0.15–0.30$), while pore size distribution and pore volume were

evaluated by Barrett–Joyner–Halenda (BJH) desorption analysis and Density Functional Theory (DFT) modelling.

Adsorption studies

Adsorption kinetics

For the kinetics study, the optimized concentration of biosorbent i.e. 2% (w/v) was added to 100 mg L^{-1} dye solution. The solution was agitated at 150 rpm at 25±2ºC for various contact times, ranging from 10 to 60 min. The adsorption capacity at equilibrium, q_e (mg g^{-1}), was calculated using Equation (2):

$$\text{Experimental } q_e \text{ (mg g}^{-1}) = \frac{(C_o - C_e)\,V}{M} \qquad (2)$$

where C_o and C_e are the initial and equilibrium dye concentration (mg L^{-1}), V is the volume of dye solution (L), and M is the biosorbent mass (g).

The experimental data were analyzed using the pseudo-first-order (PSO), pseudo-second-order (PSO), Weber-Morris intraparticle diffusion, and Elovich kinetic models to evaluate the adsorption rate and mechanism. The PFO model describes adsorption processes where the rate is proportional to the number of unoccupied sites. This model is generally associated with systems dominated by surface-controlled adsorption and is often used as an initial approach to evaluate adsorption kinetics (Nizam *et al.* 2021). The PFO kinetic equation is given by Equation (3):

$$\ln(q_e - q_t) = \ln(q_e) - k_1 t \qquad (3)$$

where q_e and q_t (mg g^{-1}) are the amount of dye adsorbed on the biosorbent at equilibrium and at time t (min), respectively. k_1 (min^{-1}) is the PFO rate constant. The PSO model assumes that

the adsorption rate is governed by interactions between the adsorbate molecules and functional groups present on the adsorbent surface. The model is frequently applied to adsorption processes involving heterogeneous adsorbents (Wang *et al.* 2019). The linear form of PSO kinetic equation is described by Equation (4):

$$\frac{t}{q_t} = \frac{1}{k_2 q_e^2} + \frac{t}{q_e} \qquad (4)$$

where q_e and q_t (mg g^{-1}) are the amount of dye adsorbed on the biosorbent at equilibrium and at time t (min), respectively. k_2 (g $mg^{-1}min^{-1}$) is the PSO rate constant. The Weber-Morris model assumes that the adsorption depends upon the diffusion of dye molecules from the solution to adsorption sites and is given by Equation (5):

$$q_t = k_{ID}\, t^{\frac{1}{2}} + C \qquad (5)$$

where q_t (mg g^{-1}) is the amount of dye adsorbed on the biosorbent at time t (min), C is the intercept related to boundary-layer thickness, and k_{ID} (mg $g^{-1}min^{-1/2}$) is the intraparticle diffusion rate constant (Nizam *et al.* 2019). The Elovich kinetic model describes chemical adsorption on an energetically heterogeneous surface and shows that adsorption decreases exponentially with an increase in surface coverage. The linear form of the model is described by Equation (6):

$$q_t = \frac{1}{\beta} \ln(\alpha\beta) + \frac{1}{\beta} \ln t \qquad (6)$$

where q_t (mg g^{-1}) is the amount of dye adsorbed on the biosorbent at time t (min), α (mg g^{-1} min^{-1}) is the initial adsorption rate, and β (g.mg^{-1}) is the surface heterogeneity constant. Model fitting was evaluated using the root mean square error (RMSE) and coefficient of determination (R^2) for linearity.

Adsorption isotherm

For the isotherm study, dye solutions of varying concentrations were treated with the same biosorbent dosage (2%, w/v) at pH 2. The mixture was agitated at 25±2ºC for 60 min. The equilibrium adsorption data were evaluated using the Langmuir, Freundlich, Temkin, and Dubinin-Radushkevich (D-R) isotherm models. These isotherms describe the relationship between the concentration of dye in a solution and the amount adsorbed onto biosorbent at a constant temperature. The Langmuir isotherm assumes monolayer adsorption onto a homogenous surface and is described by the linear equation (7):

$$\frac{1}{q_e} = \frac{1}{q_{max}} + \frac{1}{K_L C_e} \qquad (7)$$

where q_e (mg g^{-1}) is the amount of adsorbate adsorbed per unit mass of adsorbent at equilibrium, q_{max} is the maximum monolayer adsorption capacity of the adsorbent, K_L is the Langmuir adsorption constant, and C_e is the equilibrium concentration of the adsorbate in the solution (Michalak *et al.* 2013). The feasibility is indicated by the Langmuir separation factor, R_L, which is given by Equation (8):

$$R_L = \frac{1}{1 + K_L C_o} \qquad (8)$$

The Freundlich isotherm model assumes multi-layer adsorption of the dye onto a heterogeneous surface. The linear mathematical form of the Freundlich isotherm is described by Equation (9):

$$\log q_e = \log K_F + \frac{1}{n} \log C_e \qquad (9)$$

where K_F and n are the Freundlich isotherm constants related to the adsorption capacity and intensity, respectively (Michalak *et al.* 2013). Unlike the Langmuir model, which assumes a

constant adsorption energy for all sites, the Temkin model describes that the heat of adsorption decreases linearly with increasing coverage of the heterogeneous surface and is expressed by the linear Equation (10):

$$q_e = \frac{RT}{b_t} \ln C_e + \frac{RT}{b_t} \ln K_T \qquad (10)$$

where b_t is the Temkin heat constant (J mol^{-1}), K_T is the Temkin equilibrium constant (L g^{-1}), R is the universal gas constant (8.314 J $mol^{-1}K^{-1}$), and T is absolute temperature (K). The slope of the linear plot, RT/ b_t, is denoted as the Temkin constant B and reflects the degree to which the adsorption energy decreases with increasing surface coverage due to adsorbate–adsorbent interactions. The D-R isotherm describes that adsorption follows a pore-filling mechanism rather than layer-by-layer coverage of the surface. It assumes that the surface is heterogeneous with varying adsorption energies (Nizam *et al.* 2021). The linear mathematical form is given by Equation (11):

$$\ln q_e = \ln q_m - \beta\varepsilon^2 \qquad (11)$$

where q_m is the theoretical maximum adsorption capacity (mg g^{-1}), β is the activity coefficient (mol^2 J^{-2}), and the Polanyi potential, ε (J mol^{-1}),

$$= RT \ln\left(1 + \frac{1}{C_e}\right) \qquad (12)$$

The mean adsorption energy provides an insight into the nature of adsorption interactions and is given by Equation (13):

$$E\ (J\ mol^{-1}) = \frac{1}{\sqrt{2\beta}} \qquad (13)$$

Model fitting was evaluated using the root mean square error (RMSE) and coefficient of determination (R^2) for linearity.

Immobilization of biosorbent

To minimize material loss during separation and improve recovery and reusability, immobilization of the biosorbent was carried out. Initially, different ratios of sodium alginate and biosorbent were tested to obtain uniformly shaped beads with mechanical integrity. For each combination, the mechanical stability of beads was assessed by the bead-collapse method, where 50 beads of test and control each were centrifuged at 10,000 rpm for 30 min, and the number of broken beads was recorded. Based on the uniformity and bead integrity, immobilization was ultimately carried out by mixing 1.2% (w/v) sodium alginate and 15% (w/v) banana peel powder, which was then extruded dropwise into 3.5% (w/v) chilled $CaCl_2$ solution. Beads were allowed to cure in the same $CaCl_2$ solution for 3 h at 4°C and then washed thoroughly with distilled water to remove excess calcium ions. Control alginate beads, without biosorbent, were prepared similarly. Beads were stored in the refrigerator for further use.

Regeneration of immobilized biosorbent

Reusability of the immobilized banana peel biosorbent was evaluated through successive sorption–desorption cycles. After each biosorption cycle with 100 mg L^{-1} PM, dye-loaded beads were separated and treated with 0.1 N HCl or 0.1 N NaOH under constant agitation (150 rpm) for 3 h at 25±2ºC to facilitate desorption of the bound dye. The beads were then washed repeatedly with distilled water until a neutral pH was attained and reused for the subsequent sorption cycle under identical experimental conditions. Sorption–desorption experiments were performed for five consecutive cycles. After each cycle, percentage biosorption was calculated. Blank alginate beads were used as controls to account for any dye uptake by the alginate matrix. Desorption efficiency was calculated using Equation (14):

$$\text{Desorption (\%)} = \frac{\text{Amount of dye released (mg L}^{-1}\text{)}}{\text{Amount of dye initially adsorbed (mg L}^{-1}\text{)}} \times 100 \quad (14)$$

Results and discussion

Absorbance maxima of dyes

The UV-Visible spectra of aqueous solutions of both RB and PM dyes were studied between 400 to 800 nm (Figure 1). The absorbance maxima (λ_{max}) for RB was observed at 505 nm. Rit dyes, including RB, are proprietary commercial blends, as evidenced by the UV-Vis spectrum, where a broad peak is seen. Such broad spectral features are characteristic of overlapping chromophores and are commonly reported for commercial dye mixtures. Moreover, RB is marketed as an all-purpose dye capable of coloring a wide range of fabrics, including cotton, silk, and wool, which often requires the presence of multiple dye components with different affinities toward cellulosic and protein fibres (Lee *et al.* 2009). In this context, black textile dyes belonging to acid, direct, or reactive classes are well documented to possess aromatic backbones with diverse functional groups such as azo linkages, amines, and sulfonates (Kapoor *et al.* 2022; Munagapati *et al.* 2020). The peak at 505 nm is consistent with the C.I. Direct Black family of azo dyes, which have λ_{max} around 515±10 nm (Işık and Sponza 2004).

In contrast, PM is a fibre-reactive monoazo dye, belonging to the C.I. Reactive Red category, exhibiting a sharp λ_{max} at 560 nm. The result is in agreement with the previously reported λ_{max} values for Reactive Red dyes, which range from 525 to 570 nm (Karmaker *et al.* 2019; Manogaran *et al.* 2021; Oueslati *et al.* 2024). The standard graphs of the dyes showed a linear relationship between absorbance and dye concentration with R^2 values of 0.9981 and 0.9770 for RB and PM, respectively.

Effect of operational parameters

Contact time

A preliminary study was conducted to determine the effect of contact time, one of the key parameters that profoundly affects the adsorption process, using 1% (w/v) biosorbent in a 100 mg L^{-1} textile dye solution. A dye-dependent behavior of the biosorbent was observed, where banana peel showed higher biosorption efficiency for PM, and carrot peel was more effective for RB biosorption. A rapid biosorption of BRB and CRB, ranging from 65 to 70%, was observed within the first 10 min. Comparatively lower biosorption (15-25%) was seen for BPM and CPM, indicating a slower uptake during the early contact period (Figure 2a). With increasing contact time, the adsorption rate of both dyes slowed considerably, attaining equilibrium within 60 min. The availability of unoccupied adsorption sites at the initial stage facilitated rapid dye uptake, whereas at equilibrium, saturation of these sites led to repulsive interactions between the adsorbent surface and incoming dye molecules (Gupta *et al.* 2013). A similar pattern was also reported by Munagapati *et al.* (2020), where banana peel powder exhibited rapid biosorption of 100 mg L^{-1} Reactive Black 5 dye, reaching equilibrium in 180 min with an overall biosorption efficiency of ~50%. For further studies, 60 min was selected as the optimal contact time.

Biosorbent concentration

Increasing the biosorbent concentration enhances the surface area and the number of available binding sites, leading to a concentration-dependent increase in dye uptake. A similar trend has been reported previously (Kushwaha *et al.* 2014; Munagapati *et al.* 2020; Sharma and Bhalerao 2018). In the present study, comparable results were obtained (Figure 2b). BRB and CRB exhibited 70-80% biosorption at 1% biosorbent concentration, which increased to near-complete removal (~98%) at 2% concentration. Beyond 2%, the adsorption efficiency remains constant, indicating a plateau. This can be attributed to the excess concentration of biosorbent relative to the dye molecules in solution, resulting in unutilized sites (Nizam *et al.* 2021). Both

banana and carrot peel powder were equally effective in removing RB. However, for PM, banana peel powder was more effective, exhibiting an increase in dye uptake from 25% to ~70% at a concentration of 3%. CPM showed the lowest biosorption efficiency, increasing slightly to 33% at the highest tested concentration. This observation indicated differences in biosorbent–dye interactions, which were further examined through pH optimization and physicochemical analysis. For further studies, 2% was chosen as the optimal biosorbent concentration.

pH

pH is one of the most critical aspects that determine the sorption process as it affects the degree of ionization, the surface charge of the biosorbent, and the nature of the dye solution (Munagapati *et al.* 2020). However, the efficiency of dye removal has also been reported to be affected by hydrophobic interactions, hydrogen bonds, van der Waals forces, π-π interactions, and n-π interactions in aqueous solutions (Hu *et al.* 2013; Nizam *et al.* 2021; Olusegun and Mohallem 2020). Firstly, the effect of pH on the surface charge of both biosorbents was determined using the pH drift method (Daffalla *et al.* 2024). The point of zero charge (pH_{PZC}) is the pH at which the biosorbent is neutral, i.e., it has an overall zero surface charge. The surface of the biosorbents is positively charged at $pH < pH_{PZC}$, allowing biosorption of anionic dye species. At $pH > pH_{PZC}$, the surface becomes negatively charged and favors cationic dye biosorption. pH_{PZC} values for banana and carrot peel powder were 5.3 and 4.8, respectively (Figure 2c), which aligns with the previously reported values of ranging between 4.5 to 6.5 (Afolabi *et al.* 2021; Kushwaha *et al.* 2014; Mondal and Kar 2018).

The effect of pH on biosorption using banana and carrot peel powder revealed contrasting behaviors between the tested dyes (Figure 2d). The removal was consistently high across acidic pH (2–6) for both BRB and CRB, achieving nearly 100% adsorption. The sorption decreased slightly in the alkaline range. RB is a blend of multiple dye components designed

for a wide range of fabric dyeing. This is also supported by the broad UV–Vis absorption profile observed in this study. Moreover, aromatic rings with functional groups, such as azo, amine, and sulphonate moieties, are well-reported in black textile dyes (Kapoor *et al.* 2022; Munagapati *et al.* 2020). The presence of chemically diverse groups in RB enables multicomponent interactions with the biosorbent surface, thereby explaining its relatively stable biosorption behavior across a wide pH range and absence of sharp pH-dependent variation.

In contrast, BPM and CPM exhibited strong pH-dependent biosorption, with maximum removal at pH 2 (banana ~90% and carrot ~70%). Sorption declined steeply with increasing pH, reaching a minimum (~40%) at pH 8. However, an increase was observed at pH 10. Unlike RB, PM belongs to the C.I. Reactive Red monoazo dyes with prominent anionic moieties, like dichlorotriazine and sulfonic acids (Li *et al.* 2024). These anionic groups make the dye-biosorbent interactions highly sensitive to pH. For pH values less than pH_{PZC}, protonation of hydroxyl, amine, and carboxyl functional groups in both banana and carrot peels occurs, imparting an overall positive charge on the biosorbent surface (Jayesree *et al.* 2021; Khawas *et al.* 2017; Zaini *et al.* 2022). This favored electrostatic attraction with anionic dye molecules resulted in the highest uptake at pH 2, making it the optimal pH for further studies. As shown in Figure 2d, banana peel consistently showed higher uptake of PM than carrot peel across the acidic pH range, reflecting its higher biosorption efficiency.

Deprotonation at $pH > pH_{PZC}$ rendered a negative charge on the surface of biosorbents, leading to electrostatic repulsion between dye and biosorbent and, thereby, a reduction in biosorption. This also explains the lower PM uptake observed at the native pH (~6.8) during optimization of contact time and biosorbent concentration. The mechanism has been previously observed for anionic reactive dyes with banana peel and related biosorbents (Akter *et al.* 2021;

Munagapati *et al.* 2018; Tashager *et al.* 2022). The increase in biosorption of PM at pH 10 might be due to higher ionization or hydrolysis of the dye, which may expose additional moieties capable of interacting with the biosorbent (Ismail and Sakai 2024). Although the surface of biosorbent is negatively charged (pH > pH_{PZC}), adsorption can still occur through secondary mechanisms, such as hydrogen bonding, van der Waals forces, π-π interactions, and n-π interactions in aqueous solutions (Mondal and Kar 2018). Researchers have also reported that exposure to additional adsorbing sites on biomass, due to high deprotonation, increases biosorption (Achak *et al.* 2009; Zaini *et al.* 2022).

Although pH 2 yielded the highest dye removal efficiency under laboratory conditions, this value represents a mechanistic optimum, highlighting the role of surface protonation and electrostatic interactions in biosorption. Textile effluents are generally reported to exhibit pH in the range of 6–9, rather than highly acidic conditions, owing to the extensive use of alkaline chemicals during dyeing and finishing processes (Castillo-Suárez *et al.* 2023). However, in our study, appreciable dye removal (>50%) was also observed at near-neutral pH, indicating that the biosorbents retain practical applicability without extensive pH adjustment for textile effluents.

Initial dye concentration

Biosorption usually decreases with increasing initial dye concentration due to saturation of active sites on biosorbents (Akter *et al.* 2021; Daffalla *et al.* 2024; Nizam *et al.* 2021). In our study, BRB and CRB exhibited consistently high biosorption (>90%) at all the tested initial dye concentrations ranging from 50 to 150 mg L^{-1} (Figure 2e). The highest uptake of 99% was observed at a dye concentration of 100 mg L^{-1}. A slight decrease (up to 92%) due to biosorbent saturation was observed at dye concentrations above 100 mg L^{-1}.

Unlike RB, BPM and CPM exhibited distinct biosorption patterns associated with concentration gradients and mass-transfer concepts (Figure 2f). At low initial concentration, the driving force, i.e., the concentration gradient for adsorption, is weak, resulting in slow diffusion of dye molecules to the biosorbent sites in a fixed contact time. This leads to lower biosorption efficiency of 40% with carrot and 65% with banana. Increasing the initial dye concentration to 100 mg L^{-1} led to a larger concentration gradient and faster diffusion of dye molecules, creating a stronger driving force for adsorption. This resulted in an increase in dye removal to 72% and 90% with carrot and banana, respectively, indicating the higher efficiency of banana peel powder. Similar observations have also been reported for other dyes, including congo red, tartrazine azo-anionic dyes and methylene blue (Enniya and Jourani 2017; Kabbout and Taha 2014; Villabona-Ortíz *et al.* 2022). Beyond 100 mg L^{-1}, the percentage biosorption declined to 60-70% due to biosorbent saturation.

Compared with RB, PM exhibited lower biosorption with both banana and carrot peel powders. However, after optimizing biosorbent conditions, the efficiency for PM improved significantly, from ~20% pre-optimization to 90% post-optimization, indicating the influence of biosorbent concentration, pH, and contact time on dye removal efficiency.

Characterization of biosorbent before and after biosorption

FTIR analysis

The FTIR analysis of both biosorbents, before and after dye biosorption, was conducted to identify the functional groups involved in biosorption. The prominent FTIR peaks of the raw biosorbents, along with their corresponding functional groups, have been summarized in Table 1.

Banana peel biosorbent. The FTIR spectrum of raw banana peel powder (Figure 3) indicated the presence of important functional groups. A broad, intense band at 3433 cm^{-1} reflected O–H stretching vibrations of hydroxyl groups of alcohols and phenols. Dual peaks at 2918 and 2840 cm^{-1} attributed to aliphatic C–H stretching. Sharp peaks at 1737, 1454, and 1258 cm^{-1} correspond to C=O stretching of carbonyl groups, symmetric stretching of carboxylates ($-COO^-$), and C-O symmetric stretching of acidic functional groups, respectively. Presence of aromatic groups was evidenced by the C=C bending vibration at 1626 cm^{-1}, while the amide group was observed as an unresolved shoulder near 1546 cm^{-1}. A well-defined β-glycosidic linkage marker was present at 1151 cm^{-1}. The fingerprint region (below 1000 cm^{-1}) displayed seven distinct peaks, corresponding to C-H stretching and glycosidic linkages of polysaccharides, reflecting high chemical diversity and vibrational freedom of the native biomass (Akter *et al.* 2021; El Din *et al.* 2018).

After the adsorption of both PM and RB dyes onto the banana biosorbent, the spectra showed significant changes (Figure 3a,b). BRB exhibited a more pronounced increase in intensity (lower %T) across the major peaks compared to raw biosorbent, suggesting additive IR contributions from the multicomponent dye blend. Conversely, BPM showed lower intensity than banana, consistent with site-specific binding. Major chemical interactions were confirmed by significant shifts (>17 cm^{-1}) in the C-O stretching peak (from 1258 to 1234 cm^{-1} in BPM and 1241 cm^{-1} in BRB), alongside movement of the carboxylate peaks (from 1454 to 1447 cm^{-1} in BPM and 1442 cm^{-1} in BRB). The aromatic region showed significant positive shifts (>10cm^{-1}) from 1626 cm^{-1} to 1637 cm^{-1} (BPM) and 1638 cm^{-1} (BRB), confirming π–π stacking interaction. Minor shifts were also observed in the regions corresponding to hydroxyl and amine groups. Additionally, new sharp peaks at ~618 cm^{-1}, attributed to sulfonate ($–SO_3^-$) groups, confirmed the successful loading of PM and RB onto the biosorbent. Moreover, the seven peaks observed in raw biosorbent were consolidated to fewer broader signals in the

fingerprint area, indicating restricted vibrational freedom due to dye uptake. These FTIR changes confirm that dye biosorption onto banana peel occurs via a multi-modal mechanism involving: (i) hydrogen bonding, electrostatic interactions, and chemical complexation involving hydroxyl, amine, and carboxylated sites, (ii) π–π stacking interactions between the dye and aromatic rings, and (iii) surface coating.

Carrot peel biosorbent. The FTIR profile of the raw carrot biosorbent closely matched that of the banana. Intense bands observed at 3432, 2918, 2850, 1740, and 1424 cm^{-1} were attributed to hydroxyl stretching vibrations, aliphatic –CH stretching, carbonyl stretching and carboxylate vibrations. The aromatic and polyene skeletal framework was evidenced by C=C bending at 1638 cm^{-1}. Unlike raw banana peel, carrot exhibited a resolved N–H bending peak corresponding to amide of structural proteins at 1542 cm^{-1}. The O-H/C-H bending was indicated by the peak at 1383 cm^{-1}, consistent with phenolics, hydroxyl, and methyl groups. The fingerprint region (below 1000 cm^{-1}) exhibited five distinct peaks, primarily representing the polysaccharide backbone and out-of-plane aromatic vibrations (Hastuti *et al.* 2018; Jayesree *et al.* 2021).

Following biosorption (Figure 3c,d), CRB also exhibited a general increase in relative intensity (lower %T) across major bands, suggesting additive IR contributions and extensive surface loading by the dye blend. In contrast, CPM showed an attenuation in certain native bands, reflecting site-specific binding. The significant shifts were observed in the O-H/C-H bending region (from 1383 to 1377 cm^{-1} in CPM and 1376 cm^{-1} in CRB). The aromatic region exhibited a shift from 1638 cm^{-1} to 1639 cm^{-1} in both CPM and CRB, reflecting π–π stacking interactions. A shift in the carboxylate symmetric stretch (from 1424 cm^{-1} to 1423 cm^{-1} in CRB and CPM) further indicated involvement of oxygenated groups. Minor shifts were also observed for regions belonging to hydroxyl and amine groups. New sulfonate peaks near 618

cm^{-1} and reduced resolution in the fingerprint region confirmed dye loading. These changes in FTIR spectra indicate that carrot peel biosorption involves similar interaction pathways to those of banana peel, including π–π stacking, electrostatic interactions, hydrogen bonding, and surface adsorption.

Overall, both biosorbents are rich in functional groups characteristic of lignocellulosic biomass, as previously reported in banana and carrot peels. This includes cellulose, hemicellulose, lignin, pectin, carotenoids, lipids, and proteins (Akter *et al.* 2021; Memon *et al.* 2008; Oyekanmi *et al.* 2019). These groups provide appropriate binding sites for dye biosorption through a multi-modal mechanism, such as surface loading, chemical complexation, π–π stacking, electrostatic interactions, and hydrogen bonding (El Din *et al.* 2018; Hastuti *et al.* 2018; Jayesree *et al.* 2021). Moreover, a higher diversity of peaks in the fingerprint region, together with the greater magnitude of functional group shifts observed after biosorption, confirms a large number of accessible and chemically diverse binding sites in banana peel powder. This could be the plausible explanation for its higher biosorption efficiency compared to carrot, as observed during optimization studies. These results are consistent with earlier studies on fruit peel biosorbents (Shakoor and Nasar 2018).

SEM analysis

To understand the surface morphology and texture of biosorbents before and after dye biosorption, SEM imaging was performed (Figure 4).

Banana peel biosorbent. Raw banana peel powder exhibited a clear, non-uniform, and heterogeneous surface morphology with distinct edges. The presence of multiple depressions, irregular folds, cavities, and layers indicates the availability of extensive accessible surface for adsorption. These observations are similar to those reported by Tolkou *et al.* (2024). For BPM, the surface was observed to be grainy and rough, clearly showing deposition of dye molecules.

The edges were observed to be comparatively smoother. The features appeared covered with dye molecules, with partial masking of the cavities and cracks. Similar results were obtained by Hashem *et al*. (2020), where the adsorption of methylene blue on lignocellulosic fibres of banana peel waste was reported. In contrast, the BRB micrograph revealed a significant change in texture compared to the untreated banana peel. The surface appeared extensively coated with irregular clusters distributed non-uniformly across the biosorbent surface. Unlike PM, the dye accumulation was more evident within surface folds and cavities.

Carrot peel biosorbent. Untreated carrot peel powder exhibited a highly irregular, flaky, and porous surface morphology with overlapping layers, as also reported in an earlier study (Kushwaha *et al*. 2014). Compared with the banana peel, the surface of the carrot peel appeared denser, with closely packed layers available for dye uptake. Following adsorption, CPM showed localized and non-uniform changes in texture. The sharp, flaky edges of the raw biomass were covered with dye, attenuating the surface features. On the other hand, CRB showed pronounced surface loading, in which the original biosorbent structure is largely masked by unevenly distributed dye aggregates. Similar changes in surface morphology have been reported earlier in fruit peel biosorbent after the uptake of various basic and reactive dyes (Michael-Igolima *et al.*, 2023; Tolkou *et al.* 2024).

EDX analysis

EDX analysis was performed to determine the elemental composition of the biosorbents before and after dye adsorption (Figure S1). The spectra of both banana and carrot biosorbents were dominated by carbon and oxygen peaks, reflecting the lignocellulosic nature of the biomass. Other minor peaks of inorganic elements, such as K, Ca and Cl, were attributed to the mineral constituents of plant biomass. After adsorption of PM and RB dyes, additional peaks corresponding to Al, Na, and Si were observed, indicating a dye-laden biosorbent surface. Since

dyes are deposited on the biosorbent, little variation was observed in the carbon and oxygen peaks (Tolkou *et al.* 2024). These observations are consistent with our SEM results.

Surface area and pore size analysis

Table 2 summarizes the surface area, total pore volume, and average pore size of biosorbents before and after adsorption. The surface areas of banana and carrot were found to be 4.391 and 13.288 $m^2 g^{-1}$, respectively, which are comparable to earlier reports on fruit peel waste (Akmese 2025). Carrot showed higher total pore volume and lower pore size compared to banana. The N_2 adsorption–desorption isotherms of banana and carrot peel biosorbents (Figure 5) exhibited characteristics consistent with Type IV isotherms, indicating predominantly mesoporous structures typical of lignocellulosic materials (Praipipat *et al.* 2025). A gradual increase in nitrogen uptake across the entire relative pressure range, without a distinct knee at low P/P_0, reflected multilayer adsorption on heterogeneous surfaces. A more pronounced rise in adsorption at intermediate to high relative pressures ($P/P_0 > 0.4$) indicated capillary condensation within mesopores. Absence of a clear plateau further suggested the contribution of interparticle voids or external surface adsorption (Feng and Pandey 2026). Overall, the N_2 isotherm profiles of untreated biosorbents confirm that adsorption is governed by a combination of pore structure and surface heterogeneity.

Following dye adsorption, notable changes in the isotherm profiles and pore parameters were observed. Both BPM and CPM exhibited lower adsorption volumes, suggesting pore blockage and surface coverage by dye molecules, limiting accessibility of internal adsorption sites. The reduced pore size and total pore volume in BPM and CPM further confirmed this observation (Hashem *et al*. 2020). A slight increase in the surface area of BPM resulted from the surface roughness and grainy texture caused by PM deposition. In contrast, RB-loaded systems exhibited increased nitrogen uptake at higher relative pressures. This behavior could

be attributed to the dye's blended nature and its extensive loading on the biosorbent surface, resulting in multicomponent interactions and possible self-assembly of the molecules. This may lead to the formation of additional interparticle voids or a secondary mesoporous network on the biosorbent surface (Ramezani *et al.* 2024), contributing to increased pore volume and surface area (BRB) or increased average pore size (CRB).

Adsorption kinetics

The adsorption kinetics of RB and PM dyes onto banana and carrot peel biosorbents were evaluated using PFO, PSO, Weber–Morris intraparticle diffusion, and Elovich kinetic models (Table 3).

Adsorption kinetics for banana peel

For both BPM and BRB, the PSO model provided the best overall description, with a high correlation coefficient ($R^2 > 0.91$) and low RMSE (< 0.38 mg g^{-1}). Additionally, the PSO-model predicted equilibrium adsorption capacities (q_e) were close to the experimental values (Exp.q_e). Among all four systems, BPM exhibited the highest PSO rate constant ($k_2 = 4.780$ g $mg^{-1}min^{-1}$), indicating that the system approaches equilibrium rapidly. These results conclusively indicate that the adsorption rate is governed by the availability of adsorption sites on the banana rather than by dye concentration alone (Muntean *et al.* 2017; Mondal and Kar 2018). The PFO model showed very poor agreement with the experimental data, as reflected by a low R^2 value (<0.3) and a high RMSE (>2 mg g^{-1}), confirming that first-order kinetics are not suitable for describing PM and RB adsorption onto banana peel.

Weber–Morris analysis revealed a relatively high intraparticle diffusion rate constant, k_{ID} (0.10 – 0.22 mg $g^{-1}min^{-1/2}$), suggesting that the diffusion process contributes to the adsorption rate. However, the non-zero intercept values (C) indicate the boundary-layer

resistance during the early stages of adsorption, demonstrating that intraparticle diffusion is not the sole rate-limiting step. The Elovich model showed poor applicability with an unrealistically large α value for BRB, suggesting that the energetically heterogeneous chemisorption mechanism is not applicable to these systems. Overall, these observations confirm that dye adsorption on banana peel is dominated by PSO, with contributions from diffusion and boundary-layer effects.

Adsorption kinetics for carrot peel

For CPM, the PSO model outperformed the PFO model as reflected by higher correlation coefficients and lower RMSE values. The PSO rate constant for CPM (k_2 = 0.172 g $mg^{-1}min^{-1}$) was the lowest among the four systems, indicating slower adsorption kinetics. Weber–Morris analysis showed moderate correlation (R^2 = 0.777) with a non-zero intercept (C = 0.901 mg g^{-1}), suggesting that both diffusion and surface adsorption processes influence the adsorption rate. The Elovich model failed to adequately describe the kinetics (R^2 = 0.316). For CRB, PSO model again demonstrated superior performance. This system showed the highest adsorption capacity among all four systems, indicating strong and efficient dye uptake. Moreover, the PSO rate constant (k_2 = 3.188 g $mg^{-1}min^{-1}$) was substantially higher than BRB, suggesting a faster approach to equilibrium. The PFO, Weber–Morris and the Elovich analysis failed to describe the adsorption behavior, as evidenced by a low R^2 value and high RMSE.

These findings collectively indicate that adsorption of dyes proceeds via multistep mechanisms involving rapid initial uptake followed by diffusion-influenced stages, with system-specific variations depending on the dye–biosorbent combination (Agha *et al.* 2025; Michalak *et al.* 2013; Nizam *et al.* 2021).

Adsorption isotherm

The adsorption behavior of BPM, CPM, BRB and CRB was analysed using Langmuir, Freundlich, Temkin and D-R isotherm models. The parameters derived from the linear regression analysis of the models, along with their respective R^2 and RMSE values, are summarized in Table 4.

Adsorption isotherm for banana peel

BPM and BRB exhibited favorable, relatively consistent isotherm behavior. Both Freundlich ($R^2 > 0.97$; RMSE < 0.39 mg g^{-1}) and Langmuir ($R^2 > 0.96$; RMSE < 0.85 mg g^{-1}) models described the equilibrium data well, indicating dye adsorption on a heterogeneous surface with favorable intensity (n > 1.0) and a finite adsorption capacity. The separation factor, R_L, further confirmed the favorable adsorption. This suggests that although the surface is heterogeneous, adsorption on banana peel can still approach quasi-monolayer behavior under the studied conditions (Ngugi *et al.* 2016). The estimated energy value, E (0.1 to 0.5 kJ mol^{-1}) in the D-R model provided an indication of physisorption (Nizam *et al.* 2021). Temkin fitting ($R^2 = 0.839$; RMSE = 0.718 mg g^{-1}) suggested that adsorbate–adsorbent interactions influence PM adsorption on banana peel, with the Temkin constant B (2.273) indicating moderate interaction effects. However, the model fails to describe the adsorption of BRB well enough, owing to very high RMSE values compared to the best-fit Freundlich model (Esvandi *et al.* 2020).

Adsorption isotherm for carrot peel

For CPM, the Freundlich model provided an excellent fit ($R^2 = 0.989$; RMSE = 0.155 mg g^{-1}), confirming adsorption on a heterogeneous surface, although a weaker adsorption is suggested by the Freundlich adsorption capacity and intensity parameter. Langmuir fitting was moderate ($R^2 = 0.740$). Furthermore, the Temkin model showed strong conformity ($R^2 = 0.928$; RMSE = 0.321 mg g^{-1}), indicating a gradual and systematic decrease in adsorption energy with

increasing surface coverage. The Temkin constant (B = 2.033) reflects moderate interaction effects. The D–R model further supported these findings by yielding a low mean adsorption energy (E = 0.075 kJ.mol^{-1}), typically associated with physical adsorption. Thus, CPM adsorption occurs by orderly surface interactions at energetically diverse sites (Esvandi *et al.* 2020; Wang *et al.* 2019).

In contrast, CRB exhibited high biosorption efficiency in batch experiments but poor conformity to all classical adsorption isotherm models, indicating highly non-ideal equilibrium behavior. The consistently low correlation coefficients ($R^2 < 0.56$) and high RMSE values (~ 5–21 mg g^{-1}) demonstrate that the Langmuir, Freundlich, Temkin and D-R models lack predictive capability for this system and do not adequately represent a single dominant adsorption mechanism under the studied conditions. This behavior is attributed to highly irregular and multicomponent interactions between the dye blend and the non-uniform surface of carrot peel. Although studies on the uptake of dye blends via biosorption are limited, prior studies on multicomponent systems revealed both synergistic and antagonistic behavior between the components depending upon the type of adsorbate and its concentration (Wang *et al.* 2021; Zhong *et al.* 2022). None of the tested models account for the interaction between the adsorbate molecules. Moreover, the present study highlights the limitations of conventional adsorption isotherm models for adequately capturing multicomponent adsorption (Acharya *et al.* 2023).

Comparative analysis of the dye-biosorbent systems

A comparative evaluation of all four dye-biosorbent systems (BPM, BRB, CPM, and CRB) revealed distinct adsorption behaviors and mechanism dictated by both biosorbent properties and dye characteristics.

Structure and property of biosorbents

The differences in biosorbent performance across four dye-biosorbent systems highlight the role of the structural and chemical properties of the adsorbing material. Both banana and carrot peel biosorbents exhibit lignocellulosic characteristics, with FTIR confirming the presence of hydroxyl, carboxyl, amine, and aromatic functional groups, providing appropriate binding sites for dye molecules (Akter et al. 2021; Oyekanmi et al. 2019). Besides this, SEM and BET analyses revealed heterogeneous, mesoporous structures suitable for dye adsorption (Praipipat *et al.* 2025).

Although carrot peel exhibited a higher surface area and pore volume, banana peel powder demonstrated more consistent and predictable adsorption behavior, as reflected by better conformity to isotherm models. Untreated banana displayed a more heterogeneous and accessible surface morphology, characterized by folds, cavities, and irregular structures, as observed in SEM micrographs. FTIR further indicated a higher diversity of functional groups, particularly reflected in the richer fingerprint region. In contrast, carrot peel showed a comparatively denser and more compact layered structure, which may limit accessibility of internal binding sites. This suggests that adsorption is influenced not only by the surface area but also by the diversity and accessibility of functional groups (Shakoor and Nasar 2018).

Dye-dependent adsorption behavior: pure vs. blended systems

The adsorption behavior across all systems is strongly influenced by dye characteristics, which in turn dictate the dominant adsorption mechanisms and their conformity to kinetic and isotherm models. PM, a single-component reactive monoazo dye, exhibited pH-dependent and

site-specific adsorption, primarily governed by electrostatic interactions, supported by hydrogen bonding. Under acidic conditions, protonation of biosorbent surfaces enhances attraction to anionic dye molecules, leading to controlled biosorption (Afolabi et al. 2021). This is supported by moderate FTIR peak shifts, partial pore blocking in BET, and localized dye deposition in SEM, indicating adsorption at accessible active sites. Correspondingly, PM systems (BPM and CPM) followed PSO kinetics, indicating that the rate is governed by the availability of active sites (Mondal and Kar 2018), while the good fit to Freundlich and Langmuir isotherms suggests adsorption on a heterogeneous surface with quasi-monolayer characteristics (Esvandi *et al.* 2020; Ngugi *et al.* 2016). The low adsorption energy values further confirm that the process is predominantly physical in nature, involving weak interactions (Nizam *et al.* 2021).

In contrast, RB, a commercial dye blend, exhibited complex and less pH-sensitive adsorption behavior due to its multicomponent nature. The presence of diverse chromophores enables simultaneous interactions through electrostatic attraction, hydrogen bonding, π–π interactions, and van der Waals forces. This resulted in surface aggregation and clustering, as evidenced by increased FTIR band intensity (additive IR contributions), extensive surface coating and clustering in SEM, and structural modifications in BET analysis. These features are further reflected in the adsorption model behavior. While BRB conformed reasonably to isotherm models, CRB showed poor agreement with all classical models, indicating that multicomponent interactions do not align well with ideal adsorption assumptions. Such deviations from ideal behavior for blended systems do not reflect poor biosorbent performance.

Overall, the adsorption performance across systems is governed by an interplay of dye complexity, biosorbent surface chemistry, and pore structure, where multicomponent dye systems introduce additional interaction pathways and complexity beyond those observed in single-dye systems. Figure 6 illustrates the proposed adsorption mechanism of interactions

between the dye molecules and the biosorbent surface based on the characterization and adsorption studies.

Comparison with other biosorption studies

Although this is the first study on the biosorption of PM and RB using banana and carrot peel powders, both biosorbents have been investigated for the removal of other dyes. In the absence of comparative literature data for these specific dyes, previously reported adsorption capacities, optimal parameters, and percentage biosorption of banana- and carrot-derived biosorbents across various dye systems were considered for evaluation. For untreated banana peel powder, the reported adsorption capacities (q_{max}) for different dyes range from 1.7 to 24.1 mg g^{-1} (Table 5). The majority of these studies reported >90% biosorption of the dyes at acidic pH (2-3) within 120 min. In this context, the present study demonstrates comparable performance, with banana peel achieving q_{max} values of 8.7 and 10.6 mg g^{-1} for RB and PM, respectively. Additionally, 90-100 % dye uptake was observed at pH 2 within 60 min. Importantly, these results were obtained at relatively moderate dye concentrations (100 mg L^{-1}) and short contact times, indicating the rapid and effective adsorption capacity of untreated banana peel.

Several studies have also reported substantially higher q_{max} values, up to 991 mg g^{-1}, for banana-based adsorbents. However, these were achieved only after extensive modification, such as conversion to biochar, chemical activation, or combined mechanical and biological treatments (Daffalla *et al.* 2024; Hashem *et al.* 2020; Munagapati *et al.* 2020). Though these modified biosorbents were effective at removing higher dye concentrations, they also require longer contact times. In contrast, the present work demonstrates effective dye uptake using untreated banana peel, highlighting its practical relevance as a low-cost biosorbent.

Compared to banana peel, literature on dye biosorption using carrot peel–derived materials is relatively limited, with most studies focusing on heavy-metal removal, like lead,

rather than organic dyes (Hastuti *et al.* 2018). Available reports indicate that the dye adsorption capacities of carrot-based biosorbents range from 2.3 to 66.6 mg g^{-1}, depending on the nature of the dye, biomass fraction used (peel, leaves, or flower), and the treatment applied to the biomass. The adsorption capacities obtained in the present study for both dyes are within the reported range, confirming the suitability of carrot peel as a biosorbent. Also, the optimal conditions closely match those reported previously (Table 5).

The comparative evaluation suggests that both banana and carrot peel powders exhibit adsorption performance comparable to previously reported biosorption from banana and carrot wastes. The ability to achieve high dye removal using untreated materials in relatively short contact times supports the practical applicability of these biosorbents. Moreover, it also highlights the application of these biosorbents towards unreported pure reactive dye, PM and a commercial dye blend, RB, thereby reinforcing their potential for sustainable dye remediation.

Biosorption through immobilized biosorbent

Owing to its comparatively higher biosorption activity, banana peel powder was immobilized using sodium alginate. Beads of 4±1 mm size were formed using 15% biosorbent mixed with 1.2% alginate. None of the beads collapsed at 10,000 rpm for 30 min, indicating their good mechanical strength, stability, and structural integrity under high centrifugal force. Figure 7 shows the sorption-desorption efficiency of immobilized banana beads regenerated using 0.1 N HCl and 0.1 N NaOH across successive cycles. Blank alginate beads without the biosorbent served as a control and showed negligible dye sorption.

With HCl as the desorbing agent, the biosorption efficiency increased progressively from 55% during the first cycle to 90% in the third cycle. Most studies report a gradual decrease in dye uptake due to incomplete desorption or structural degradation of beads (Atiba-Oyewo

et al. 2019; Ramírez-Rodríguez *et al.* 2023). In the present study, the increase in biosorption during initial HCl regeneration cycles is atypical and has been previously attributed to a surface-cleaning or conditioning effect. Mild acid treatment facilitates the removal of impurities, pore-blocking substances, and residual calcium ions, thereby improving the accessibility of the binding sites on the immobilized biosorbent (Hu and Hu 2013). The decline in biosorption in the fourth and fifth cycles may result from partial exhaustion of binding sites or weakening of the alginate-biosorbent matrix after repeated acid washing.

Desorption efficiency with HCl remained consistently low (2-15%) across all cycles, comparable to the findings of Reyes-Ledezma *et al.* (2020), where a maximum of 12% desorption of anionic dye was observed under acidic pH. This suggests dye-biosorbent interactions, predominantly through electrostatic attractions and hydrogen bonding with diverse functional groups of biosorbent. Our FTIR data confirmed the involvement of hydroxyl, amine, carbonyl and carboxyl functional groups for dye adsorption (Figure 3). The results are also consistent with our pH-optimization studies, which demonstrate improved uptake of anionic PM under acidic conditions. A similar trend has been reported for anionic dye Acid Orange II adsorption systems, operated under acidic conditions, where adsorption capacity increased over the initial cycles and reached a maximum before declining (Wang *et al.* 2021). In this study, adsorption was favored at pH 2, while desorption required alkaline conditions (pH 11). This behavior supports the present observations, where acidic conditions enhanced PM adsorption but limited its release during HCl regeneration, resulting in low desorption efficiencies.

On the contrary, regeneration with NaOH was observed to be 47% during the first cycle, which is much higher than that with HCl. This indicates successful disruption of dye-biosorbent interactions and effective regeneration of the immobilized biosorbent. A similar observation

was reported by Reyes-Ledezma *et al.* (2020), where alkaline conditions were proposed to promote electrostatic repulsion by rendering negative charges on the biosorbent surface, leading to the elution of anionic dyes. However, a steep decline in sorption efficiency was observed in the second cycle due to matrix degradation. At high pH, the alginate matrix swells due to the exchange of gel cations with the sodium ions in solution. This results in loss of cross-linkages and release of encapsulated material (Abka-Khajouei *et al.* 2022; Ching *et al.* 2017), thereby compromising the integrity of the beads. Therefore, although alkaline treatment is effective for desorption, it is not suitable for repeated regeneration as it adversely affects the stability and integrity of the alginate-biosorbent matrix. These contrasting behaviors observed with HCl and NaOH regeneration demonstrate that regeneration efficiency alone does not guarantee biosorbent reusability, highlighting the importance of balancing desorption efficiency with structural and functional stability. Overall, our results indicate that the banana peel alginate beads are reusable and maintain their adsorption efficiency over multiple cycles.

Conclusions

This study represents the first comparative investigation of the removal of pure (PM) vs. blended (RB) commercial textile dyes using banana and carrot peel waste as effective biosorbents, highlighting distinct adsorption behaviors in single-component and blended-dye systems. Optimization of operational parameters significantly enhanced biosorption efficiency, achieving 70–100% dye removal. The maximum adsorption capacity of BRB, BPM, CRB, and CPM reached 8.7, 10.6, 36.6 and 11.4 mg g^{-1}, respectively, reflecting the differences in dye-biosorbent affinity. The dye removal is driven by functional group-mediated interactions between dye and biosorbent, prominently with aromatic rings, hydroxyl, carboxyl and amine groups. The FTIR band intensification after RB biosorption is attributed to extensive surface loading of the dye blend, as also confirmed by SEM. While pure PM systems follow more

predictable and model-conforming adsorption pathways, blended RB systems introduce additional mechanistic complexity, leading to deviations from ideal adsorption behavior. This highlights the limitations of conventional adsorption models in describing multi-component blended dyes. Immobilized banana peel maintained high biosorption efficiency over multiple regeneration cycles, demonstrating its potential for repeated application.

Overall, this work presents a sustainable, low-cost, and eco-friendly biosorption approach that not only effectively removes textile dyes but also promotes waste valorization by utilizing domestic fruit and vegetable residues. The study demonstrates strong adsorption performance under optimized conditions; however, it is important to note that the experiments were conducted at a constant temperature with synthetic dye solutions, which may not fully capture the complexity and variability of real textile effluents. Future studies incorporating temperature-dependent experiments for thermodynamic evaluation, post-regeneration characterization of immobilized biosorbents with FTIR, SEM-EDX, and mass-loss measurements are warranted to provide an in-depth understanding of adsorption, long-term biosorbent stability, and practical applicability. Moreover, phytotoxicity assessment of untreated and treated effluents could provide valuable insights into the environmental safety and sustainability of the biosorption process.

Acknowledgements

The authors thank the Sophisticated Analytical Instrument Facility (SAIF), IIT Bombay, for FTIR analysis. The authors also acknowledge support from The Central Research Facility, IIT Jodhpur, and Diya Labs, Mumbai, for SEM-EDX and BET analysis.

Supplementary Material

Figure S1 illustrates the EDX analysis of banana and carrot biosorbents before and after adsorption of PM and RB textile dyes.

Author contributions

CRediT: Samiksha Patil: Methodology, Investigation, Formal analysis, Visualization, Writing – original draft; Richa Singh: Conceptualization, Supervision, Visualization, Validation, Writing – review and editing

Disclosure statement

No potential conflict of interest was reported by the author(s).

Declaration of funding

No funding was received.

Data availability statement

The data that support the findings of this study are available from the corresponding author, [RS], upon reasonable request.

References

Abka-Khajouei R, Tounsi L, Shahabi N, Patel AK, Abdelkafi S, Michaud P. 2022. Structures, properties and applications of alginates. Mar Drugs. 20:364. doi: 10.3390/md20060364.

Achak M, Hafidi A, Ouazzani N, Sayadi S, Mandi L. 2009. Low-cost biosorbent "banana peel" for the removal of phenolic compounds from olive mill wastewater: Kinetic and equilibrium studies. J Hazard Mater. 166:117–125. doi: 10.1016/j.jhazmat.2008.11.036.

Acharya A, Jeppu G, Girish CR, Prabhu B. 2023. Development of a multicomponent adsorption isotherm equation and its validation by modeling. Langmuir. 39:17862–17878. doi: 10.1021/acs.langmuir.3c02496.

Afolabi FO, Musonge P, Bakare BF. 2021. Bio-sorption of a bi-solute system of copper and lead ions onto banana peels: characterization and optimization. J Environ Health Sci Eng. 19(1):613–624. doi: 10.1007/s40201-021-00632-x.

Agha HM, Jawad AH, Wilson LD, AlOthman ZA. 2025. Adsorptive performance of sustainable biosorbent from *Macadamia integrifolia* shell powder for methylene blue dye removal: desirability functions and uptake mechanism. Int J Phytoremediation. 27:1287–1302. doi: 10.1080/15226514.2025.2494697.

Ahmed AE, Majewska-Nowak K. 2020. Removal of reactive dye from aqueous solutions using banana peel and sugarcane bagasse as biosorbents. Environ Prot Eng. 46:121–135. doi: 10.37190/epe200308.

Akkari I, Graba Z, Bezzi N, Merzeg FA, Bait N, Ferhati A, Kaci MM. 2024. Biosorption of Basic Red 46 using raw cactus fruit peels: equilibrium, kinetic and thermodynamic studies. Biomass Convers Biorefin. 14:1825–1836. doi: 10.1007/s13399-022-02354-y.

Akmese, B. 2025. Removal of brilliant blue R and victoria blue R dyes from textile wastewater by adsorption method using pomegranate peel. BMC Chem. 19: 99. doi: 10.1186/s13065-025-01476-4.

Akpomie KG, Conradie J. 2020. Banana peel as a biosorbent for the decontamination of water pollutants: A review. Environ Chem Lett. 18:1085–1112. doi: 10.1007/s10311-020-00995-x.

Aksu Z. 2005. Application of biosorption for the removal of organic pollutants: a review. Process Biochem. 40:997–1026. doi: 10.1016/j.procbio.2004.04.008.

Akter M, Rahman FBA, Abedin MZ, Kabir SMF. 2021. Adsorption characteristics of banana peel in the removal of dyes from textile effluent. Textiles. 1(2):361–375. doi: 10.3390/textiles1020018.

Atiba-Oyewo O, Onyango MS, Wolkersdorfer C. 2019. Synthesis and application of alginate immobilised banana peels nanocomposite in rare earth and radioactive minerals removal from mine water. IET Nanobiotechnol. 13:756–765. doi: 10.1049/iet-nbt.2018.5399.

Bouchelkia N, Mouni L, Belkhiri L, Bouzaza A, Bollinger JC, Madani K, Dahmoune F. 2016. Removal of lead (II) from water using activated carbon developed from jujube stones, a low-cost sorbent. Sep Sci Technol. 51:1645–1653. doi: 10.1080/01496395.2016.1178289.

Castillo-Suárez LA, Sierra-Sánchez AG, Linares-Hernández I, Martínez-Miranda V, Teutli-Sequeira EA. 2023. A critical review of textile industry wastewater: green technologies for the removal of indigo dyes. Int J Environ Sci Technol. 20:10553–10590. doi: 10.1007/s13762-023-04810-2.

Chahal M, Kumari S, Bhattacharya A, Garg MC. 2024. Evaluating sustainable agricultural waste biomass for methylene blue adsorption in wastewater treatment: A state-of-the-art review. Bioresour Technol Rep. 28:101983. doi: 10.1016/j.biteb.2024.101983.

Ching SH, Bansal N, Bhandari B. 2017. Alginate gel particles: a review of production techniques and physical properties. Crit Rev Food Sci Nutr. 57:1133–1152. doi: 10.1080/10408398.2014.965773.

Daffalla SB, Taha AA, Da'na EAM, El-Aassar MR. 2024. Sustainable banana-waste-derived biosorbent for Congo Red removal from aqueous solutions: kinetics, equilibrium, and breakthrough studies. Water. 16:1449. doi: 10.3390/w16101449.

Djama C, Bouguettoucha A, Chebli D, Amrane A, Tahraoui H, Zhang J, Mouni L. 2023. Experimental and theoretical study of methylene blue adsorption on a new raw material, *Cynara scolymus*—a statistical physics assessment. Sustainability. 15:10364. doi: 10.3390/su151310364.

El-Din GA, Amer AA, Malsh G, Hussein M. 2018. Study on the use of banana peels for oil spill removal. Alexandria Eng J. 57:2061–2068. doi: 10.1016/j.aej.2017.05.020.

Elsisi H, Elmaaty TA, Negm E, Abouelenin S. 2025. Dyeing wool fabrics with specialized dyes and their mixtures using supercritical CO_2. Sci Rep. 15:40377. doi: 10.1038/s41598-025-25134-w.

Enniya I, Jourani A. 2017. Study of methylene blue removal by a biosorbent prepared with apple peels. J Mater Environ Sci. 8:4573–4581.

Esvandi Z, Foroutan R, Peighambardoust SJ, Akbari A, Ramavandi B. 2020. Uptake of anionic and cationic dyes from water using natural clay and clay/starch/$MnFe_2O_4$ magnetic nanocomposite. Surf Interfaces. 21:100754. doi: 10.1016/j.surfin.2020.100754.

Feng R, Pandey R. 2026. Multiscale evaluation of nanopore architecture and fractal geometry in shale reservoirs. GeoEnergy Communications. 2(1):2. doi: 10.1007/s44421-025-00012-3.

Girija A, Mareeswaran PM. 2023. Toxicity analysis of dyes. In: Mareeswaran PM, Rajesh J, editor(s). Advances in Dye Degradation. Singapore: Bentham Science Publisher. p. 33-50.

Gómez-Aguilar DL, Rodríguez-Miranda JP, Salcedo-Parra OJ. 2022. Fruit peels as a sustainable waste for the biosorption of heavy metals in wastewater: A review. Molecules. 27:2124. doi: 10.3390/molecules27072124.

Gupta S, Prajapati A, Kumar A. 2025. Removal of anionic dyes by magnetic modified *A. barbadensis Miller* residue leaves as a bio-adsorbent using biosorption process. Green Technol Sustain. 3:100196. doi: 10.1016/j.grets.2025.100196.

Gupta VK, Pathania D, Sharma S, Agarwal S, Singh P. 2013. Remediation and recovery of methyl orange from aqueous solution onto acrylic acid grafted *Ficus carica* fiber: Isotherms, kinetics and thermodynamics. J Mol Liq. 177:325–334. doi: 10.1016/j.molliq.2012.10.007.

Hashem AH, Saied E, Hasanin MS. 2020. Green and ecofriendly bio-removal of methylene blue dye from aqueous solution using biologically activated banana peel waste. Sustain Chem Pharm. 18:100333. doi: 10.1016/j.scp.2020.100333.

Hastuti B, Totiana F, Winiasih R. 2018. The role of pectin in Pb binding by carrot peel biosorbents: isotherm adsorption study. IOP Conf Ser: Mater Sci Eng. 349:012011. doi: 10.1088/1757-899X/349/1/012011.

Hemashenpagam N, Selvajeyanthi S. 2023. Textile dyes and their effect on human beings. In: Ahmad A, Jawaid M, Ibrahim MNM, Yaqoob AA, Alshammari MB, editor(s). Nanohybrid materials for treatment of textile dyes. Singapore: Springer Nature. p. 41-60.

Homdi TA, Akhtar K, Bakhsh EM, Fagieh TM, Alhemadan AH, Khan SB. 2024. Design of low-cost recyclable adsorbent based on cellulosic bags filled with carbon black derived from carrot peels for water remediation. Sustain Chem Pharm. 38:101499. doi: 10.1016/j.scp.2024.101499.

Hu SH, Hu SC. 2013. Pyrolysis of paper sludge and utilization for ionic dye adsorption. Bioresources. 8:1028–1042.

Hu Y, Guo T, Ye X, Li Q, Guo M, Liu H, Wu Z. 2013. Dye adsorption by resins: Effect of ionic strength on hydrophobic and electrostatic interactions. Chem Eng J. 228:392–397. doi: 10.1016/j.cej.2013.04.116.

Ibrahim NA. 2011. Dyeing of textile fibre blends. In: Clark M, editor. Handbook of Textile and Industrial Dyeing. Cambridge (UK): Woodhead Publishing. p. 147–172. doi: 10.1533/9780857093974.1.147.

Işık M, Sponza DT. 2004. Monitoring of toxicity and intermediates of CI Direct Black 38 azo dye through decolorization in an anaerobic/aerobic sequential reactor system. J Hazard Mater. 114:29–39. doi: 10.1016/j.jhazmat.2004.06.011.

Islam MT, Islam T, Islam T, Repon MR. 2022. Synthetic dyes for textile colouration: Process, factors and environmental impact. Textile Leather Rev. 5:327–373. doi: 10.31881/tlr.2022.27.

Ismail GA, Sakai H. 2024. pH-dependent dye protonation and the effect of iron on dye degradation during Fenton-based processes. Ozone Sci Eng. 46:294–308. doi: 10.1080/01919512.2023.2285690.

Jayesree N, Hang PK, Priyangaa A, Krishnamurthy NP, Ramanan RN, Turki MA, Charis MG, Ooi CW. 2021. Valorisation of carrot peel waste by water-induced hydrocolloidal complexation for extraction of carotene and pectin. Chemosphere. 272:129919. doi: 10.1016/j.chemosphere.2021.129919.

Kabbout R, Taha S. 2014. Biodecolorization of textile dye effluent by biosorption on fungal biomass materials. Phys Procedia. 55:437–444. doi: 10.1016/j.phpro.2014.07.063.

Kapoor RT, Rafatullah M, Siddiqui MR, Khan MA, Sillanpää M. 2022. Removal of reactive black 5 dye by banana peel biochar and evaluation of its phytotoxicity on tomato. Sustainability. 14(7):4176. doi: 10.3390/su14074176.

Karmaker S, Sintaha F, Saha TK. 2019. Kinetics, isotherm and thermodynamic studies of the adsorption of reactive red 239 dye from aqueous solution by chitosan 8B. Adv Biol Chem. 9:1-22. doi: 10.4236/abc.2019.91001.

Khawas P, Das AJ, Deka SC. 2017. Banana peels and their prospects for industrial utilization. In: Anal AK, editor(s). Food Process By-Products Their Utilization. New Jersey (USA): John Wiley & Sons. p.195–206.

Kumari S, Agarwal S, Kumar M, Sharma P, Kumar A, Hashem A, Abd-Allah EF, Garg MC. 2025. An exploration of RSM, ANN, and ANFIS models for methylene blue dye adsorption using *Oryza sativa* straw biomass: a comparative approach. Sci Rep. 15:2979. doi: 10.1038/s41598-025-87274-3.

Kumari S, Singh R, Jahangeer J, Garg MC. 2024. Innovative strategies for dye removal from textile wastewater: A comprehensive review of treatment approaches and challenges. Water Air Soil Pollut. 235:720. doi: 10.1007/s11270-024-07532-4.

Kushwaha AK, Gupta N, Chattopadhyaya MC. 2014. Removal of cationic methylene blue and malachite green dyes from aqueous solution by waste materials of *Daucus carota*. J Saudi Chem Soc. 18(3):200–207. doi: 10.1016/j.jscs.2011.06.011.

Lee CH, Sun TK, Lin RF, Chen HS, inventors; Everlight USA Inc., assignee. 2009 April 28. Black dye composition and black ink composition for textile digital printing. United States patent US 7,524,368.

Li D, Ma W, Tang B, Zhang S. 2024. Excellent fixation and color fastness of nylon fibers dyed with low-water-soluble reactive dyes based on the reactivity and stability of vinyl sulfone. Textile Res J. 94:259–273. doi: 10.1177/004051752311958.

Manogaran M, Yasid NA, Othman AR, Gunasekaran B, Halmi MIE, Shukor MYA. 2021. Biodecolourisation of Reactive Red 120 as a sole carbon source by a bacterial consortium-Toxicity assessment and statistical optimisation. Int J Environ Res Public Health. 18(5):2424. doi: 10.3390/ijerph18052424.

Mehra S, Singh M, Chadha P. 2021. Adverse impact of textile dyes on the aquatic environment as well as on human beings. Toxicol Int. 28(2):165-176. doi: 10.18311/ti/2021/v28i2/26798.

Memon JR, Memon SQ, Bhanger MI, Memon GZ, El-Turki A, Allen GC. 2008. Characterization of banana peel by scanning electron microscopy and FT-IR spectroscopy and its use for cadmium removal. Colloids Surf B Biointerfaces. 66(2):260–265. doi: 10.1016/j.colsurfb.2008.07.001.

Meretoudi AD, Kalampogias I, Koumentakou I, Kalavrouziotis IK, Tolkou AK, Kyzas GZ. 2025. Chitosan/montmorillonite/graphene oxide composites for the adsorption of dyes from single-component solutions, binary mixtures, and real textile wastewaters: understanding the adsorption interactions. Langmuir. 41:23198–23213. doi: 10.1021/acs.langmuir.5c03148.

Michalak I, Chojnacka K, Witek-Krowiak A. 2013. State of the art for the biosorption process—a review. Appl Biochem Biotechnol. 170(6):1389–1416. doi: 10.1007/s12010-013-0269-0.

Michael-Igolima U, Abbey SJ, Ifelebuegu AO, Eyo EU. 2023. Modified orange peel waste as a sustainable material for adsorption of contaminants. Materials. 16(3):1092. doi: 10.3390/ma16031092.

Mondal NK, Kar S. 2018. Potentiality of banana peel for removal of Congo red dye from aqueous solution: isotherm, kinetics and thermodynamics studies. Appl Water Sci. 8(6):157. doi: 10.1007/s13201-018-0811-x.

Moradi R, Kashefi AM, Marandi R, Salahi E, Moradi DS. 2021. Application of Box–Behnken design and response surface methodology of Acid Red 18 adsorption onto Fe_3O_4-coated carrot waste PAC: kinetic and isotherm studies. Arch Hyg Sci. 10:30–48. doi: 10.52547/archhygsci.10.1.30.

Munagapati VS, Wen JC, Pan C-L, Gutha Y, Wen J-H, Reddy GM. 2020. Adsorptive removal of anionic dye (Reactive Black 5) from aqueous solution using chemically modified banana peel powder: kinetic, isotherm, thermodynamic, and reusability studies. Int J Phytoremediation. 22(3):267–278. doi: 10.1080/15226514.2019.1658709.

Munagapati VS, Yarramuthi V, Kim Y, Lee KM, Kim DS. 2018. Removal of anionic dyes (Reactive Black 5 and Congo Red) from aqueous solutions using banana peel powder as an adsorbent. Ecotoxicol Environ Saf. 148:601–607. doi: 10.1016/j.ecoenv.2017.10.075.

Muntean SG, Todea A, Bakardjieva S, Bologa C. 2017. Removal of non-benzidine direct red dye from aqueous solution by using natural sorbents: beech and silver fir. Desalination Water Treat. 66:235–250. doi: 10.5004/dwt.2016.0154.

Nasra E, Kurniawati D, Etika SB, Silvia R, Rahmatika A. 2021. Effect of pH and concentration on biosorption of malachite green and rhodamine B dyes using banana peel (*Musa balbisiana Colla*) as biosorbent. J Phys Conf Ser. 1788:012003. doi: 10.1088/1742-6596/1788/1/012003.

Ngugi F, Onyari JM, Wabomba JN. 2016. Efficacy of mangrove (*Rhizophora mucronata*) root powder in adsorption of lead (II) ions from aqueous solutions: equilibrium and kinetics studies. IOSR J Appl Chem. 9:45–51. doi: 10.9790/5736-0908024551.

Nizam NUM, Hanafiah MM, Mahmoudi E, Halim AA, Mohammad AW. 2021. The removal of anionic and cationic dyes from an aqueous solution using biomass-based activated carbon. Sci Rep. 11(1):8623. doi: 10.1038/s41598-021-88084-z.

Olusegun SJ, Mohallem ND. 2020. Comparative adsorption mechanism of doxycycline and Congo red using synthesized kaolinite supported $CoFe_2O_4$ nanoparticles. Environ Pollut. 260:114019. doi: 10.1016/j.envpol.2020.114019.

Oueslati K, Kyzas GZ, Naifar A, Lamine AB. 2024. Understanding the adsorption of Reactive Red 2 onto metal hydroxide sludge: analysis with physico-statistical steric and energetic perspectives. Environ Sci Pollut Res. 31(25):37824–37834. doi: 10.1007/s11356-024-33753-5.

Oyekanmi AA, Ahmad A, Hossain K, Rafatullah M. 2019. Adsorption of Rhodamine B dye from aqueous solution onto acid-treated banana peel: response surface methodology, kinetics and isotherm studies. PLoS One. 14(5):e0216878. doi: 10.1371/journal.pone.0216878.

Peng H, Guo J. 2020. Removal of chromium from wastewater by membrane filtration, chemical precipitation, ion exchange, adsorption, electrocoagulation, electrochemical reduction, electrodialysis, electrodeionization, photocatalysis and nanotechnology: a review. Environ Chem Lett. 18:2055–2068. doi: 10.1007/s10311-020-01058-x.

Pokharia AP, Ahluwalia SS. 2015. Toxicological effect of textile dyes and their metabolites: A review. Curr Trend Biotechnol Chem Res. 5(1):11–17.

Praipipat P, Ngamsurach P, Bunchu K, Lekwaree V. 2025. Methylene blue removal using zinc and magnesium oxides doped banana peels: Isotherm, kinetics and mechanism. Environ Chem Ecotoxicol. 7:729-740. doi: 10.1016/j.enceco.2025.04.005

Raji Z, Maleka R, Karim A, Karam A, Aider M, Khalloufi S. 2025. Biosorption of lead from water using fruit and vegetable peels: characteristics, adsorption kinetics, and isotherms. Int J Environ Sci Technol. 22:15775–15790. doi: 10.1007/s13762-025-06667-z.

Ramezani P, De Smedt SC, Sauvage F. 2024. Supramolecular dye nanoassemblies for advanced diagnostics and therapies. Bioeng Transl Med. 9(4): e10652. doi: 10.1002/btm2.10652.

Ramírez-Rodríguez AE, Cristiani-Urbina E, Morales-Barrera L, Aranda-García E. 2023. Continuous successive cycles of biosorption and desorption of acid red 27 dye using water hyacinth leaves as an effective, economic, and ecofriendly biosorbent. Bioprocess Biosyst Eng. 46(2):183–193. doi: 10.1007/s00449-022-02822-9.

Reyes-Ledezma JL, Uribe-Ramírez D, Cristiani-Urbina E, Morales-Barrera L. 2020. Biosorptive removal of acid orange 74 dye by HCl-pretreated *Lemna* sp. PLoS One. 15:e0228595. doi: 10.1371/journal.pone.0228595.

Rit Dye. 2025. Black: All purpose dye – Rit Dye. Illinois (US):Nakoma Products; [accessed 2025 Oct 30]. https://www.ritdye.com/products/black/

Shakoor S, Nasar A. 2018. Utilization of *Punica granatum* peel as an eco-friendly biosorbent for the removal of methylene blue dye from aqueous solution. J Appl Biotechnol Bioeng. 5(4):242–249. doi: 10.15406/jabb.2018.05.00145.

Shamshad J, Rehman RU. 2025. Innovative approaches to sustainable wastewater treatment: a comprehensive exploration of conventional and emerging technologies. Environ Sci Adv. 4:189-222. doi: 10.1039/d4va00136b.

Sharma AS, Bhalerao SA. 2018. Application of immobilized banana peels (*Musa paradisiaca L.*) into calcium alginate beads for removal of chromium (VI) from aqueous solution. Int J Trend Sci Res Dev. 2:1310-1325. doi: 10.31142/ijtsrd9665.

Singh D, Singh D, Mishra V, Kushwaha J, Sengar M, Sinha S, Singh S, Giri BS. 2024. Strategies for biological treatment of wastewater: A critical review. J Clean Prod. 454:142266. doi: 10.1016/j.jclepro.2024.142266.

Singha K, Pandit P, Maity S, Sharma SR. 2021. Harmful environmental effects of textile chemical dyeing practice. In: Ibrahim N, Hussain CM, editor(s). Green chemistry for sustainable textiles. Cambridge (MA):Woodhead Publishing, Elsevier. p. 153-164.

Swamy MM, Nagabhushana BM, Krishna RH, Kottam N, Raveendra RS, Prashanth PA. 2017. Fast adsorptive removal of methylene blue dye from aqueous solution onto wild carrot flower

activated carbon: isotherms and kinetics studies. Desalin Water Treat. 71:399–405. doi: 10.5004/dwt.2017.20520.

Teshager FM, Habtu NG, Mequanint K. 2022. A systematic study of cellulose-reactive anionic dye removal using a sustainable bioadsorbent. Chemosphere. 303(Pt 2):135024. doi: 10.1016/j.chemosphere.2022.135024.

Thabede PM, Shooto ND. 2025. Removal of methyl orange from water using biochar derived from a blend of carrot and potato peels. Desalin Water Treat. 324:101584. doi: 10.1016/j.dwt.2025.101584.

Tolkou AK, Tsoutsa EK, Kyzas GZ, Katsoyiannis IA. 2024. Sustainable use of low-cost adsorbents prepared from waste fruit peels for the removal of selected reactive and basic dyes found in wastewaters. Environ Sci Pollut Res Int. 31:14662-14689. doi: 10.1007/s11356-024-31868-3.

Vievard J, Alem A, Pantet A, Ahfir ND, Arellano-Sánchez MG, Devouge-Boyer C, Mignot M. 2023. Bio-based adsorption as an eco-friendly method for wastewater decontamination: a review. Toxics. 11(5):404. doi: 10.3390/toxics11050404.

Villabona-Ortíz Á, Figueroa-Lopez KJ, Ortega-Toro R. 2022. Kinetics and adsorption equilibrium in the removal of azo-anionic dyes by modified cellulose. Sustainability. 14(6):3640. doi: 10.3390/su14063640.

Wang H, Zhang J, Zhu J, Chang J, Wang N, Chen H. 2021. Synergistic and antagonistic effects and mechanisms of Cr(VI) adsorption and reduction by Fe(III)–humic acid coprecipitates. J Hazard Mater. 409:124529. doi: 10.1016/j.jhazmat.2020.124529.

Wang J, Zhang W, Kang X, Zhang C. 2019. Rapid and efficient recovery of silver with nanoscale zerovalent iron supported on high-performance activated carbon derived from straw biomass. Environ Pollut. 255:113043. doi: 10.1016/j.envpol.2019.113043.

Wang W, Hu J, Zhang R, Yan C, Cui L, Zhu J. 2021. A pH-responsive carboxymethyl cellulose/chitosan hydrogel for adsorption and desorption of anionic and cationic dyes. Cellulose. 28:897–909. doi: 10.1007/s10570-020-03561-4.

Yarik S, Bouaifel FB, Bezzi N, Akkari I, Kessi S, Bouaouina K. 2025. Adsorption of methylene blue by lemon verbena leaf waste: valorization, decontamination and modeling. Environ Monit Assess. 197:768. doi: 10.1007/s10661-025-14223-y.

Yaseen DA, Scholz M. 2019. Textile dye wastewater characteristics and constituents of synthetic effluents: A critical review. Int J Environ Sci Technol. 16:1193–1226. doi: 10.1007/s13762-018-2130-z.

Yasmeen N, Munir R, Albasher G, Mushtaq N, Younas F, Zahid M, Aliyam T, Noreen S. 2025. Biosynthesis of *Daucus carota subsp. Sativus*-based metal-doped ferric–biochar–bimetallic nanocomposites for dye extraction. Chem Pap. 79:1113–1135. doi: 10.1007/s11696-024-03845-0.

Zaini HM, Roslan J, Saallah S, Munsu E, Sulaiman NS, Pindi W. 2022. Banana peels as a bioactive ingredient and its potential application in the food industry. J Funct Foods. 92:105054. doi: 10.1016/j.jff.2022.105054.

Zhong Y, Wang K, Guo C, Kou Y, Hassan A, Lu Y, Wang J, Wang W. 2022. Competitive adsorption of malachite green and rhodamine B on polyethylene and polyvinyl chloride

microplastics in aqueous environment. Water Sci Technol. 86:894–908. doi: 10.2166/wst.2022.252.

Table 1. FTIR peaks of raw biosorbent and their corresponding functional groups

Functional groups	**Wavenumber (cm^{-1})**	
	Banana	**Carrot**
-OH stretching (hydroxyl)	3433	3432
-CH stretching (aliphatic)	2918, 2840	2918, 2850
C=O stretching (carbonyl)	1737	1740
C=C bending (aromatic)	1626	1638
N-H bending (amide)	Unresolved	1542
COO- stretching (carboxylate)	1454	1424
C-H or O-H bending (phenolics)	1383	1383
C-O stretching (ester/acid)	1258	1258
C-O-C stretching (glycosidic)	1151	Unresolved
C-O stretching	1033	1032
Fingerprint region (β-linkages, out of plane C-H vibrations)	< 1000	< 1000

Table 2. Surface analysis of biosorbent before and after dye uptake

Parameters	**Banana**	**BPM**	**BRB**	**Carrot**	**CPM**	**CRB**
BET surface area (m^2/g)	4.391	5.187	11.312	13.288	7.397	8.537
Total pore volume ($x10^{-3}$ cc/g)	3.365	2.728	7.316	7.477	2.415	8.135
Average pore radius (nm)	1.532	1.052	1.293	1.125	0.652	1.906

Table 3. Parameter values for adsorption kinetic models for RB and PM

Model	Parameter	BPM	BRB	CPM	CRB
	Exp. q_e (mg g^{-1})	2.555	7.097	1.774	8.207
Pseudo-first-order	q_e (mg g^{-1})	0.772	0.294	0.713	0.458
	k_1 (min^{-1})	0.013	0.035	0.024	0.023
	RMSE (mg g^{-1})	2.009	7.419	1.446	9.559
	R^2	0.159	0.295	0.963	0.240
Pseudo-second- order	q_e (mg g^{-1})	2.089	7.153	1.730	8.084
	k_2 (g.$mg^{-1}min^{-1}$)	4.780	0.205	0.172	3.188
	RMSE (mg g^{-1})	0.375	0.070	0.154	0.236
	R^2	0.924	0.999	0.966	0.998
Weber-Morris intraparticle diffusion	k_{ID} (mg $g^{-1}min^{-½}$)	0.214	0.106	0.101	0.065
	C	0.879	6.304	0.901	7.669
	RMSE (mg g^{-1})	0.202	0.035	0.081	0.237
	R^2	0.763	0.952	0.777	0.175
Elovich	α (mg $g^{-1}min^{-1}$)	4.511	5.392×10^{11}	34.401	1.890×10^{15}
	β	2.882	4.587	5.618	5.000
	RMSE (mg g^{-1})	0.274	0.089	0.159	0.206
	R^2	0.289	0.688	0.316	0.256

Table 4. Parameter values for adsorption isotherm models for RB and PM

Model	Parameter	BPM	BRB	CPM	CRB
Langmuir	q_m (mg g^{-1})	10.616	8.696	11.428	36.630
	K_L	0.011	0.014	0.004	0.104
	R_L	0.468	0.410	0.729	0.088
	RMSE (mg g^{-1})	0.805	0.438	0.505	6.732
	R^2	0.964	0.982	0.740	0.526
Freundlich	K_F	0.128	0.129	0.005	7.610
	n	1.104	1.199	0.651	2.559
	RMSE (mg g^{-1})	0.381	0.205	0.155	6.967
	R^2	0.977	0.996	0.989	0.379
Temkin	K_T	0.143	0.578	0.064	1.686
	B	2.273	4.475	2.033	7.171
	RMSE (mg g^{-1})	0.718	6.347	0.321	20.790
	R^2	0.839	0.816	0.928	0.300
Dubinin-Radushkevich	q_m (mg g^{-1})	3.589	7.972	2.667	27.248
	E (kJ mol^{-1})	0.158	0.500	0.075	0.354
	RMSE (mg g^{-1})	1.260	1.257	0.618	5.804
	R^2	0.692	0.745	0.878	0.554

Table 5. Comparative assessment of banana and carrot-based biosorbents for dye removal

Adsorbent	Dyes	q_{max} (mg g^{-1})	Optimal dye conc. (mg L^{-1}), pH, time (min)	Removal (%)	Reference
I. Based on Banana					
Banana peel	Congo red	1.7	20-50, 10, 90	75	Mondal and Kar 2018
Banana peel (biochar)	Reactive black 5	7.6	75, 3, 120	96	Kapoor *et al.* 2022
Banana peel	Malachite green	8.1	100, 3, --	--	Nasra *et al.* 2021
Banana peel	Black azabache	**8.7**	100, 2, 60	~100	**Present study**
Banana peel	Rhodamine B	9.5	200, 2, 60	~90	Oyekanmi *et al.* 2019
Banana peel	Procion magenta	**10.6**	100, 2, 60	90	**Present study**
Banana peel	Rhodamine B	16.9	100, 3, --	--	Nasra *et al.* 2021
Banana peel	Reactive black 5	21.2	150, 3, 180	--	Munagapati *et al.* 2018
Banana peel	Eurozol navy blue	24.1	50, 7, 60	68-72	Ahmed *et al.* 2020
Banana peel (biochar)	Congo red	35.5	20-100, 3, 120	66-89	Daffalla *et al.* 2024
Banana peel (chemically modified)	Reactive black 5	211.8	400, 3, 180	--	Munagapati *et al.* 2020
Banana peel (pretreated & activated)	Methylene blue	991.0	--	--	Hashem *et al.* 2020
II. Based on Carrot					
Carrot peel (carbon black)	Acridine orange	2.3	40, 6, 180	92	Homdi *et al.* 2024
Carrot peel	Procion magenta	**11.4**	100, 2, 60	70	**Present study**
Carrot flower activated carbon	Methylene blue	21.0	5-10, 6, 30	60-90	Swamy *et al.* 2017
Carrot peel	Black azabache	**36.6**	100, 2, 60	~100	**Present study**
Carrot waste (PAC coated with nanoparticles)	Acid Red 18	41.0	100, 3, 80	99.7	Moradi *et al.* 2021
Carrot waste (leaves)	Malachite green	52.6	10, 7, 30	75	Kushwaha *et al.* 2014
Carrot + potato peels (biochar)	Methyl orange	56.4	100, 2, 120	--	Thabede and Shooto 2025
Carrot waste (leaves)	Methylene blue	66.6	10, 7, 30	87	Kushwaha *et al.* 2014

Note: -- (Not reported)

Figure legends

Figure 1. (a) UV-Visible spectrum of PM and RB showing absorbance maxima at 505 and 560 nm, respectively. Calibration graphs of (b) PM and (c) RB recorded at their respective λ_{max} with regression equation and correlation coefficient (R^2) value for linearity. The experiments were conducted in triplicate and the values are expressed as mean ± s.d.

Figure 2. Effect of key parameters on biosorption of PM and RB. (a) contact time (min), (b) biosorbent concentration (%, w/v), (c) Point of zero charge (pH_{PZC}) of biosorbents, (d) pH, and (e,f) initial concentration (mg L^{-1}). The optimization experiments were conducted in triplicate and the values are expressed as mean ± s.d.

Figure 3. FTIR spectra of biosorbent before and after dye biosorption. (a) BPM, (b) BRB, (c) CPM, (d) CRB. Peak shifts observed after biosorption are highlighted in red.

Figure 4. SEM micrographs of (a) untreated banana, (b) BPM, (c) BRB, (d) untreated carrot, (e) CPM and (f) CRB, illustrating surface morphology before and after biosorption. Dye deposition and morphological changes after biosorption are indicated by the arrow.

Figure 5. N_2 adsorption–desorption isotherms of (a) banana and (b) carrot peel biosorbents before and after adsorption of PM and RB dyes.

Figure 6. Proposed adsorption mechanism of PM and RB dyes on banana and carrot peel biosorbents illustrating (a) π–π stacking interactions between aromatic rings, (b) electrostatic attraction, (c) hydrogen bonding, (d) surface deposition and dye aggregation and (e) pore diffusion and filling within the biosorbent matrix.

Figure 7. Biosorption-desorption efficiency of immobilized banana peel beads regenerated using (a) 0.1 N HCl, and (b) 0.1 N NaOH. The experiments were conducted in triplicate and the values are expressed as mean ± s.d.

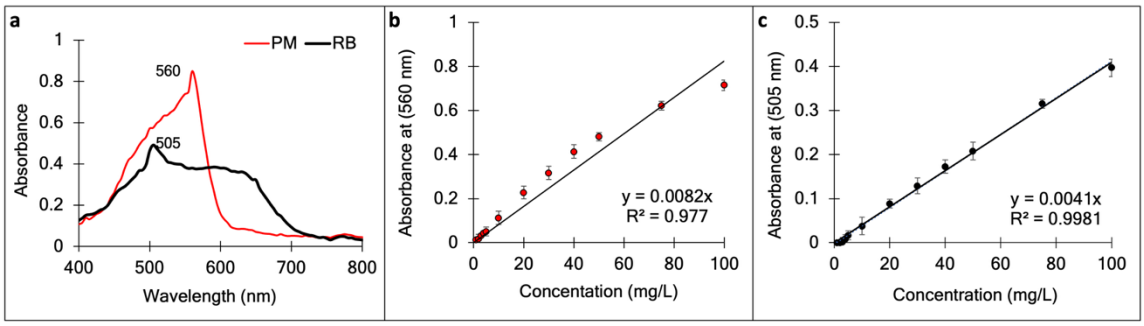

Figure 1

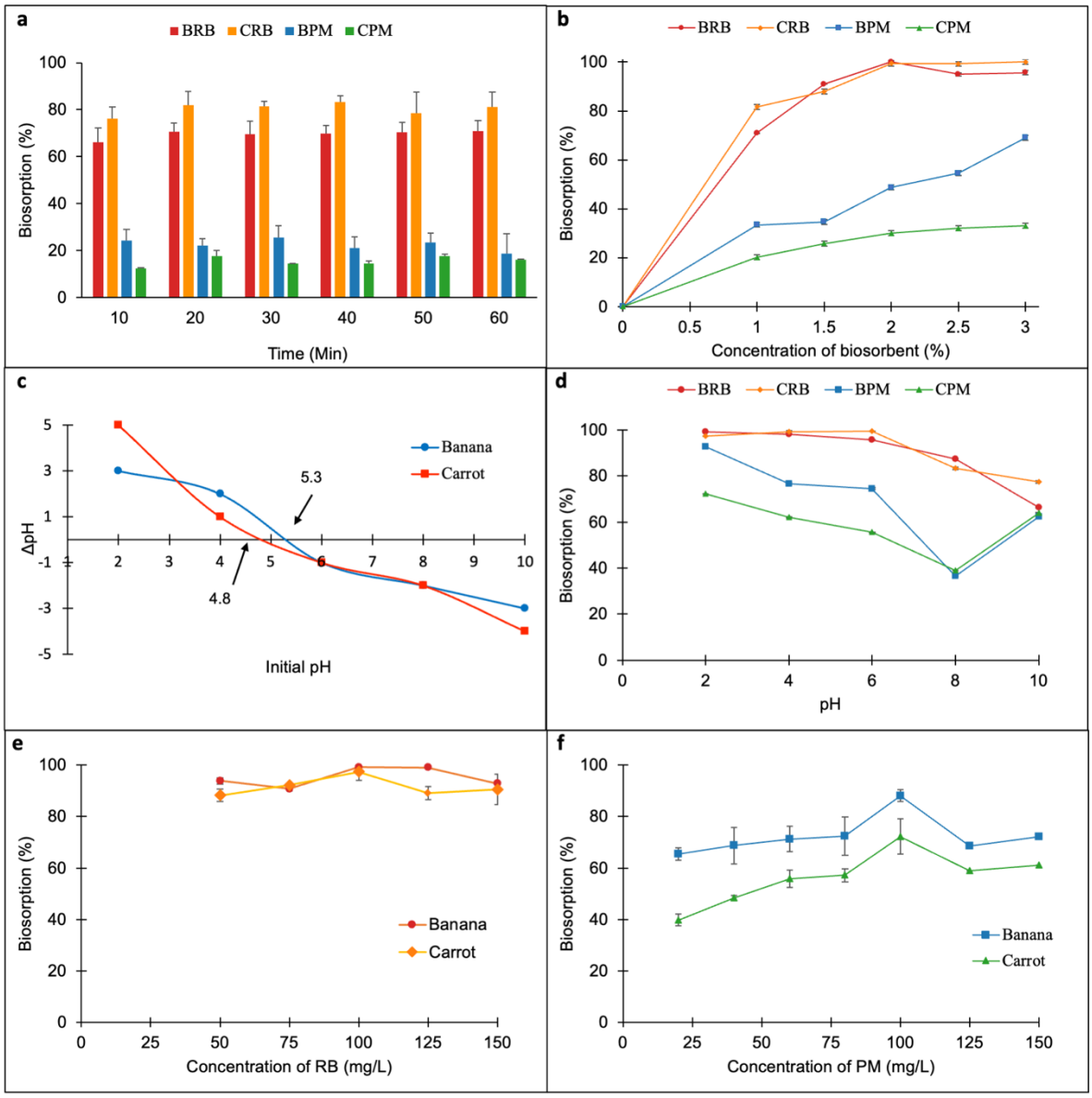
a
BRB CRB BPM CPM
Biosorption (%)
Time (Min)
b
BRB CRB BPM CPM
Biosorption (%)
Concentration of biosorbent (%)
c
Banana
Carrot
5.3
4.8
ΔpH
Initial pH
d
BRB CRB BPM CPM
Biosorption (%)
pH
e
Banana
Carrot
Biosorption (%)
Concentration of RB (mg/L)
f
Banana
Carrot
Biosorption (%)
Concentration of PM (mg/L)

Figure 2

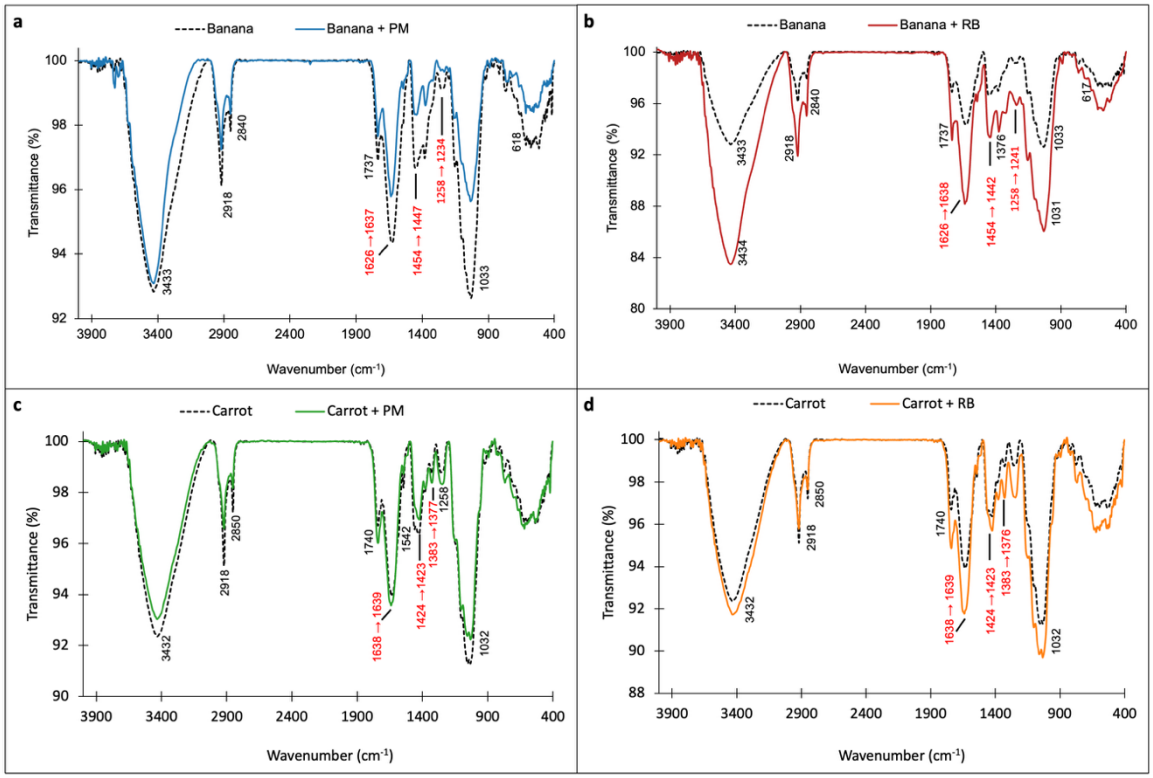

Figure 3

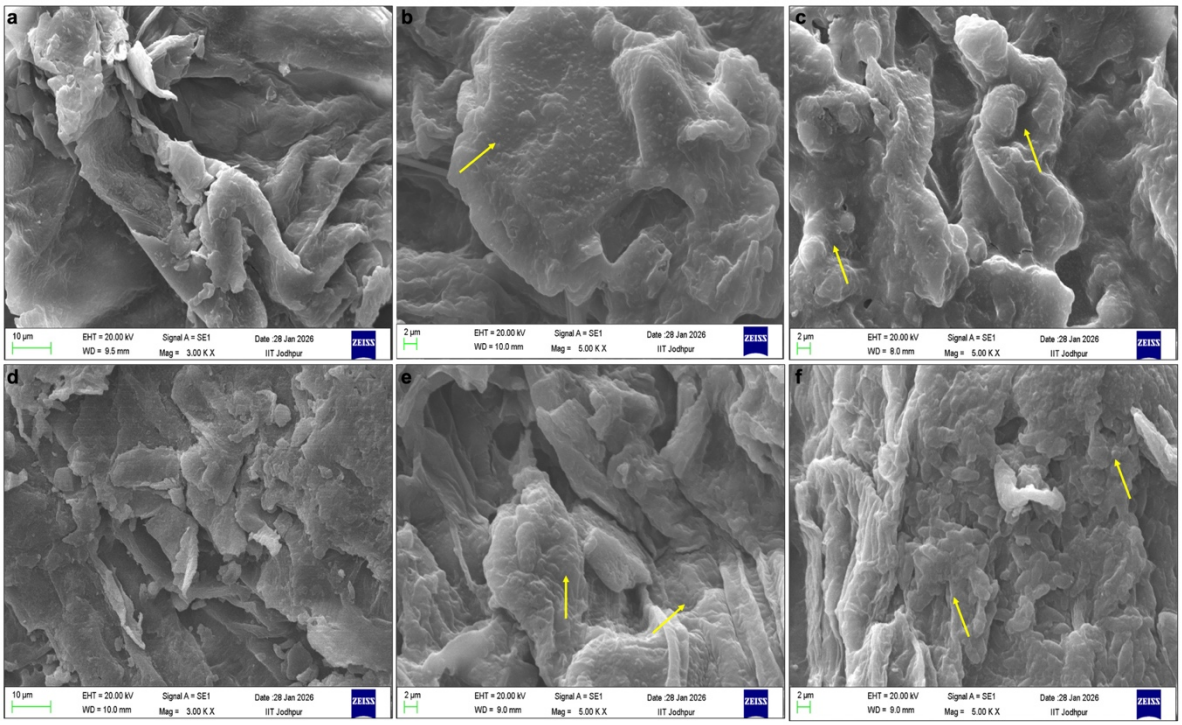

Figure 4

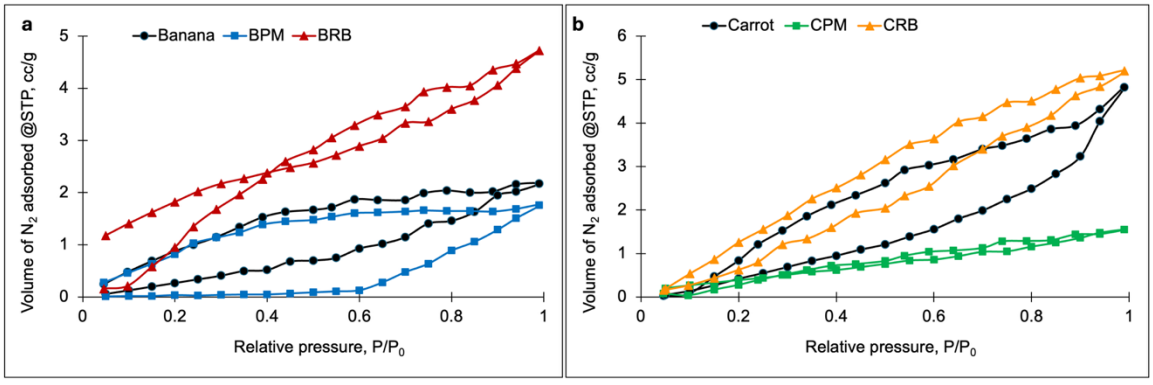

Figure 5

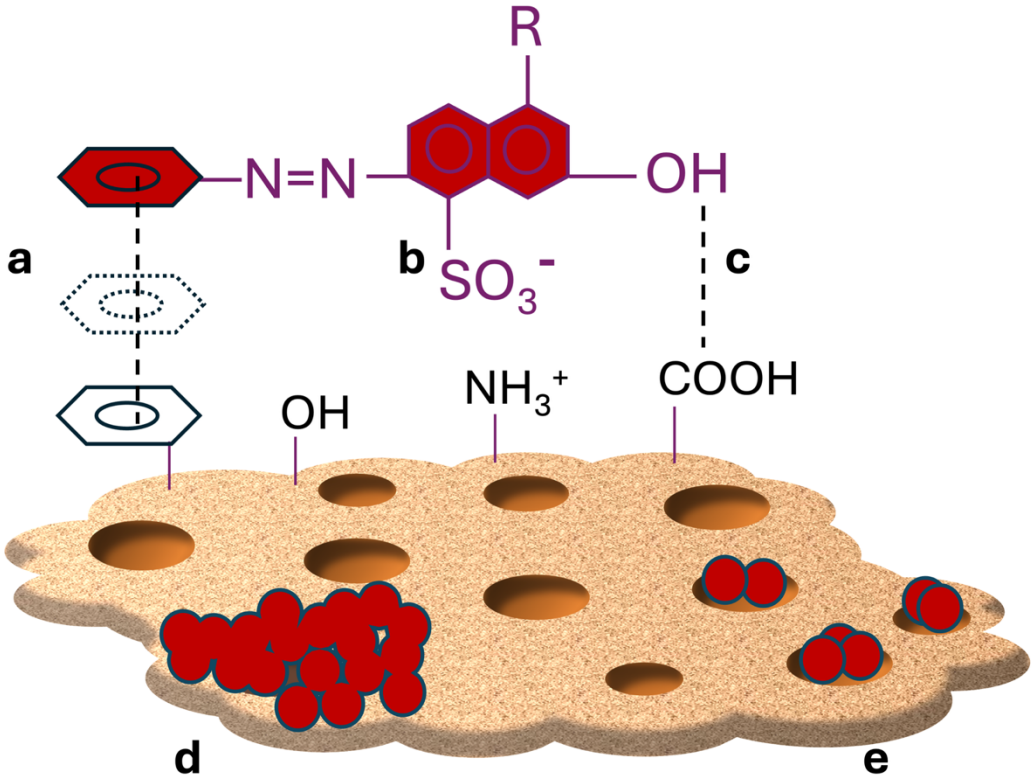

Figure 6

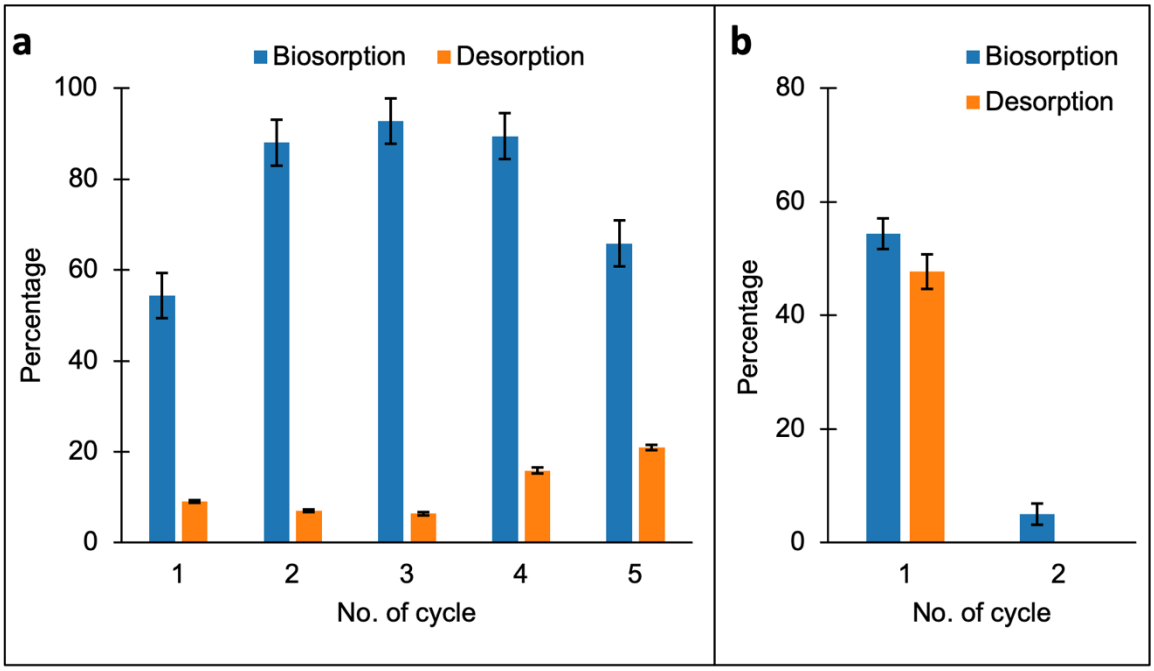

Figure 7